

Press Hardening of Advanced
High-Strength Steels:
Process development and characterisation

Khalifa Maissara

Engineering Materials

Press Hardening of Advanced High-Strength
Steels: *Process development and
characterisation*

Khalifa Maissara

Doctoral Thesis

Engineering Materials

Division of Materials Science

Department of Engineering Sciences and Mathematics

Luleå University of Technology

June 2026

*Dedicated to my mother, Khadija Rahmouni
& my father, Hassan Maissara*

*“And my success is not but through Allah. Upon Him I have relied,
and to Him I return.”*

(Quran 11:88)

Preface

This PhD work was carried out at the Division of Materials Science, Department of Engineering Sciences and Mathematics, Luleå University of Technology (LTU). The research was conducted within the framework of the project “Pro-Chain”, a collaboration among SSAB, Scania/Traton, Gestamp HardTech, and LTU, administered by the Centre for High Performance Steels (CHS) at LTU. The financial support provided by SSAB and Scania/Traton is gratefully acknowledged.

I am especially thankful to my supervisor, Marta-Lena Antti, for your generous support, trust, and encouragement during this journey. Your guidance in structuring the work and keeping things on track has been invaluable. Special thanks to my co-supervisor, Farnoosh Forouzan, for always being available despite the distance and for your openness to long in-depth discussions and the unconditional support during this project. Many thanks to my co-supervisor, Pia Åkerfeldt, for your kindness and support throughout this period. I truly appreciate the thoughtful feedback and the way you approach challenges, and your willingness to help. I would also like to thank my co-supervisor, Paul Åkerström, for your valuable input, time for long discussions, and support in this project. A special thanks to Ilana Timokhina for your assistance and for always being so helpful, providing critical feedback and suggestions. A special acknowledgement to Esa Vuorinen, who inspired me to continue working with steel.

A special thanks to Jenny Fritz (SSAB), Lars Troive (SSAB), Henrik Sieurin (Scania/Traton), and Katarina Eriksson (Gestamp HardTech), our industrial partners, for fruitful discussions during our project meetings.

Lars Frisk and Erik Nilsson, a big thank you for all your help. Your expertise during the training sessions and your assistance with the lab equipment are greatly appreciated. Thanks to colleagues from solid mechanics, Erik Lundholm, Simon Jonsson, Fredrik Larsson, Jan Granström, Erik Olsson, and Jörgen Kajberg, for their help with the mechanical testing and for the nice discussions. Also, I am grateful to Daniel Casellas and his team at Eurecat in Manresa for the nice collaborations and fruitful meetings.

Big THANK YOU to my wonderful colleagues in the Materials Science, PhDs and postdocs, especially Janna, Rahman, and Patricio, for creating such a positive and friendly working environment. A kind thank you to Birgit, Ida, Latifa, Kumar, Farid, Johanne, and Wangzhong for the happy moments and chats during this journey. I feel incredibly lucky to have such amazing friends around me: Nasir, Abdellatif, Talha, Hamza, Abdulsalam, Hesham, Mohamed, Abu Jaafar, Hamid, Amin, and Abdallah. Your unwavering support and kindness throughout my PhD journey mean so much to me. A shoutout to my friends in Morocco, especially Youssef, Hesham, Abderrazzak, Hamid, Anas, and Abdelmonaim, who have always been super supportive.

Lastly, I would like to express my sincere gratitude to my beloved Mother, Khadija, and Father, Hassan. Words cannot fully express my gratitude for their constant support, unconditional love and encouragement. This achievement would not have been possible without their prayers and sacrifices. I would also like to express my gratitude to my beloved brothers, Youness and Mohamed, and sisters, Majda and Fatima, and all family members.

Khalifa Maissara

June 2026, Luleå

Abstract

Press hardening is a thermomechanical process that enables the production of ultra-high-strength steel components with complex geometries and superior crash performance, making it essential for lightweight automotive structures. The final properties of press-hardened steels are governed by a sequence of coupled phenomena, including austenitization, hot deformation of austenite, phase transformation during cooling, and subsequent low-temperature thermal treatments. While these relationships are relatively well established for conventional 1.5 GPa grades such as 22MnB5, the underlying mechanisms in next-generation 2.0 GPa steels remain insufficiently explored. This lack of knowledge limits the ability to accurately predict microstructural evolution and optimise industrial press hardening processes for these advanced materials.

The aim of this thesis was to investigate how microstructural evolution governs the performance of ultra-high-strength steels for press hardening applications, with a particular focus on commercially available 2.0 GPa grades benchmarked against conventional 1.5 GPa steels. The influence of post-quench thermal treatments, including tempering, auto-tempering, and paint baking, on martensitic microstructures and mechanical performance was evaluated. A low-temperature tempering regime (180-200 °C) effectively enhanced yield strength while preserving the high tensile strength and good ductility of the martensitic microstructure. In contrast, higher tempering temperatures (250-300 °C) promoted martensite recovery and carbide coarsening, leading to a pronounced reduction in strength and the onset of tempered martensite embrittlement. The implications of these microstructural changes for fracture resistance were further examined by considering the effects of baking treatment and prior austenite grain size. Fracture toughness was found to be strongly governed by carbon content, with the 2.0 GPa grade exhibiting significantly lower resistance to crack propagation compared to the 1.5 GPa steel. The paint baking treatment enhanced fracture toughness in both steels, with a more pronounced improvement in the higher-strength grade. In addition, prior austenite grain size exerted a secondary but systematic influence, where finer grain structures provided consistently higher resistance to crack propagation. The effect of thermomechanical processing was investigated through simulations of press hardening conditions using Gleeble testing. The results demonstrated that deformation of austenite significantly altered phase transformation kinetics,

where increasing strain and decreasing deformation temperature accelerated diffusive transformations, resulting in a reduced martensite fraction in the final microstructure. Austenite grain growth was modelled, and the effects of austenitization temperature and holding time on bending performance were also investigated. The developed grain growth model predicted the evolution of grain size under conditions of homogeneous growth. The results indicated that austenitization temperature has no significant effect on bending performance for short holding times, while only a minor reduction in bending performance was observed at longer austenitization times. Finally, transformation mechanisms beyond conventional martensitic pathways were explored through the study of quenching and partitioning treatments in a high-silicon steel using in-situ high-energy synchrotron X-ray diffraction. The findings demonstrated that pre-existing martensite accelerates carbide-free bainitic transformation by promoting nucleation and affecting carbon partitioning, providing insight into alternative microstructure design strategies with potential relevance for press hardening applications.

In summary, this thesis establishes comprehensive process-structure-property relationships across the press hardening value chain, providing a foundation for improved process design, predictive modelling, and the development of ultra-high-strength steels with enhanced performance.

Table of Contents

Chapter 1 Introduction	1
1.1 Research background	1
1.2 Aim of the work.....	4
1.3 Research questions	4
1.4 List of appended papers.....	5
Chapter 2 Literature Review.....	7
2.1 Advanced high-strength steels and processing.....	7
2.1.1 Press hardening process	7
2.1.2 Metallurgical aspects of press hardening steels	9
2.1.3 Quenching and partitioning.....	19
2.2 Phase transformation during thermomechanical processes.....	23
2.2.1 Effect of deformation parameters	24
2.3 Fracture toughness.....	25
2.3.1 Linear elastic fracture mechanics.....	26
2.3.2 Elastic-plastic fracture mechanics.....	27
2.4 Modelling austenite grain growth.....	28
Chapter 3 Materials and Methods.....	31
3.1 Materials	31
3.2 Processes.....	31
3.2.1 Quenching and tempering	32
3.2.2 Press hardening	32
3.2.3 Bake hardening.....	33
3.2.4 Quenching and partitioning.....	33
3.3 Gleeble simulations	34

3.4	Microstructural characterisation.....	36
3.5	Mechanical characterisation.....	37
3.5.1	Uniaxial tensile test.....	37
3.5.2	Fracture toughness test.....	37
3.5.3	Three-point bending.....	38
3.5.4	Hardness.....	38
Chapter 4	Summary of Appended Papers.....	39
4.1	Paper I.....	39
4.2	Paper II.....	40
4.3	Paper III.....	42
4.4	Paper IV.....	43
4.5	Paper V.....	44
Chapter 5	Conclusions and Future Work.....	47
5.1	Conclusions.....	47
5.2	Future work.....	49
References	53
Appended papers	67

Chapter 1 Introduction

1.1 Research background

Modern engineering structures increasingly rely on materials that combine high mechanical strength with reliable in-service performance. In sectors such as the automotive industry, the demand for reduced vehicle weight, improved crash performance, and lower exhaust emissions has driven the development and widespread use of advanced high-strength steels (AHSS). Vehicle lightweighting plays a key role in this context, as a reduction in structural mass directly contributes to lower fuel consumption and, consequently, reduced carbon dioxide emissions over the vehicle's lifetime [1].

Within the vehicle architecture, the body-in-white (BIW) represents a major contributor to the overall mass, accounting for approximately 30% of the vehicle's total weight [2]. As a result, the BIW offers significant potential for weight reduction through material and design optimisation. To achieve this, modern BIW structures increasingly employ a multi-material approach, combining different metallic materials to meet local performance requirements [3]. Even though conventional steels exhibit a higher mass density compared to alternative lightweight materials such as aluminium and magnesium alloys, steel remains highly competitive due to its favourable strength-to-weight ratio. In particular, the substitution of thick, low-strength steels with thinner sections of AHSS enables substantial weight reduction while maintaining or even enhancing the structural integrity and crash performance of the vehicle.

AHSS represents a broad family of steels that have been progressively developed to meet increasing performance demands in automotive applications. Based on their microstructural concepts and mechanical response, AHSS are commonly classified into several generations, reflecting the evolution of alloy design and processing strategies over time [4]. The first generation of AHSS, introduced in the 1990s, is characterised by multiphase microstructures containing martensite in combination with one or more additional phases. This generation includes several widely used grades, typically classified according to their tensile strength lev-

els. Dual-phase (DP) steels, consisting of a ferritic matrix with dispersed martensite islands, offer improved formability compared to conventional high-strength steels due to their favourable strain-hardening behaviour. Complex-phase (CP) steels, which contain bainite in addition to ferrite and martensite, provide enhanced strength while retaining reasonable formability. Transformation-induced plasticity (TRIP) steels further improve ductility by incorporating retained austenite, which transforms to martensite during deformation and thereby increases strain hardening and elongation [5].

In addition to these cold-formable grades, the first generation also includes martensitic (MART) steels produced by cold forming, as well as press-hardening steels (PHS) formed at elevated temperatures [4]. These steels exhibit predominantly martensitic microstructures and achieve very high strength levels, making them particularly suitable for safety-critical structural components. However, as strength increases, challenges related to reduced ductility and damage tolerance become increasingly pronounced.

The second generation of AHSS comprises steels with fully austenitic microstructures at room temperature, such as twinning-induced plasticity (TWIP) steels and austenitic stainless (AUST SS) steels. These materials exhibit exceptional formability and high strength, enabled by deformation mechanisms such as mechanical twinning. Despite their attractive mechanical properties, the widespread use of second-generation AHSS in automotive structures remains limited due to their high alloying content, associated material costs, weldability challenges, and susceptibility to delayed cracking [6].

In response to the limitations of both first- and second-generation AHSS, a third generation of AHSS has been developed with the aim of achieving a more optimal balance between strength, ductility, and industrial feasibility. This generation includes concepts such as quenching and partitioning (Q&P) steels, carbide-free bainite (CFB) steels, and medium-manganese steels [7]. A common feature among these materials is the stabilisation of retained austenite, which enhances strain hardening and delays the onset of localised deformation. Despite their promising mechanical performance, however, third-generation AHSS, such as Q&P steels, face challenges related to practical implementation at the industrial

scale. In particular, the complexity of heat-treatment schedules and the sensitivity of the resulting microstructures to process parameters may limit their compatibility with high-volume automotive production lines [7,8]. Consequently, there is a strong interest in developing processing routes that are not only effective in stabilising retained austenite, but also sufficiently short and robust to meet industrial requirements. Achieving this goal requires a detailed understanding of microstructural evolution during the process.

While third-generation AHSS offers significant advances, hot forming of press-hardening steels remains the dominant industrial solution for achieving ultra-high strength levels in safety-critical components [9]. A representative example is the widely used 22MnB5 steel, which reaches a tensile strength of approximately 1.5 GPa after press hardening. Driven by increasingly strict environmental regulations and the continued demand for vehicle lightweighting, there is growing interest in the development of press-hardening steels with even higher strength levels, extending toward 2.0 GPa [10]. In parallel with these mechanical demands, passenger safety remains a central design requirement, placing increased emphasis on material performance beyond tensile strength alone. As strength levels increase, the ability to maintain an adequate balance between strength, ductility, and fracture toughness becomes a key challenge. This balance may be partially addressed through the application of tailored heat-treatment strategies, such as quenching and tempering, which offer pathways to modify the martensitic microstructure and improve damage tolerance while retaining high strength.

Furthermore, the thermomechanical conditions employed during manufacturing, including deformation at high temperature, can significantly influence transformation kinetics and the resulting microstructure. While the effect of deformation on phase transformation behaviour has been studied for press-hardening steels with strength levels around 1.5 GPa, corresponding investigations at strength levels approaching 2.0 GPa remain limited [11,12]. Addressing this is essential for the development and validation of predictive models used to simulate hot stamping processes, particularly with respect to microstructural evolution and resulting mechanical behaviour.

1.2 Aim of the work

The aim of this thesis was to investigate how microstructure evolution affects the performance of ultra-high-strength steels that can be used in press hardening applications. Particular focus has been on commercially available steels with a strength level of 2.0 GPa (~ 0.34 wt.% C), benchmarking to the commonly used 1.5 GPa grade (~ 0.24 wt.% C). In addition, the potential of the Q&P process for improving microstructural control in press hardening applications is investigated.

To achieve the aim, the following objectives were defined:

- To quantify the effect of different tempering and auto-tempering conditions on the microstructural and mechanical performance.
- To investigate how thermomechanical processing affects prior austenite characteristics, phase transformation kinetics, and the final microstructure-property relationship.
- To study transformation kinetics, phase evolution and carbon partitioning during Q&P treatment in comparison with austempering in a high silicon steel, with a specific focus on the role of pre-existing martensite in accelerating carbide-free bainitic transformation using in-situ HE-XRD.

1.3 Research questions

The following three research questions were formulated:

1. How do tempering and auto-tempering influence the tensile properties and fracture toughness of different grades of press-hardening steels?
2. How do austenitization parameters and prior austenite deformation influence the evolution of parent austenite and its impact on phase transformation and mechanical performance in press-hardening steels?
3. How does pre-existing martensite influence the kinetics and mechanism of carbide-free bainitic transformation during quenching and partitioning heat treatment?

1.4 List of appended papers

1. Khalifa Maissara, Farnoosh Forouzan, Pia Åkerfeldt, Ilana Timokhina, Paul Åkerström, Esa Vuorinen, Marta-Lena Antti. Effect of tempering on microstructure and tensile properties of ultra-high strength steels for press hardening applications. *Metallurgical and Materials Transactions A*. 2025 May 16:1-6.
2. Khalifa Maissara, Simon Larsson, Farnoosh Forouzan, Erik Olsson, Pia Åkerfeldt, Paul Åkerström, Ilana Timokhina, Marta-Lena Antti. Effect of paint baking on the fracture resistance of a 2 GPa press-hardened steel used in automotive applications. *Submitted to Materials Processing Technology*.
3. Khalifa Maissara, Farnoosh Forouzan, Paul Åkerström, Pia Åkerfeldt, Ilana Timokhina, Marta-Lena Antti. Effect of thermomechanical treatment on phase transformation kinetics during press hardening process. *Manuscript*.
4. Erik Lundholm, Khalifa Maissara, Paul Åkerström. The influence of austenitization conditions on grain growth and the bending performance of boron steel. *Metallurgical and Materials Transactions B*. 2025 Nov 24:1-2.
5. Khalifa Maissara, Farnoosh Forouzan, Roohallah Surki Aliabad, Emad Maawad, Esa Vuorinen. Influence of pre-existing martensite on the acceleration of carbide-free bainite transformation studied by in-situ synchrotron XRD. *Under review in Materials Today Communications*.

Papers not included in the thesis

1. Khalifa Maissara, Farnoosh Forouzan, Pia Åkerfeldt, Paul Åkerström, Esa Vuorinen, Marta-Lena Antti. Microstructural characterisation and tensile fracture behaviour of PHS2000 in comparison with PHS1500. The 9th International Conference on Hot Sheet Metal Forming of High-Performance Steel (CHS2), Nashville, United States, May 27–29, 2024 (pp. 409-415). *Association for Iron and Steel Technology, AISTECH*.
2. Khalifa Maissara, Farnoosh Forouzan, Esa Vuorinen. Real-time synchrotron measurement of microstructural evolution during quenching and partitioning: insights for optimizing Q&P within press hardening. The 10th International

Conference on Hot Sheet Metal Forming of High-Performance Steel (CHS2), Plzen, Czech Republic, June 1–3, 2026. *Accepted for publication in conference proceedings.*

Chapter 2 Literature Review

This chapter provides the scientific background relevant to the topics addressed in this thesis. It summarises key concepts related to press hardening, phase transformations, and microstructure-property relationships. Parts of this chapter build upon background material previously developed in the author's licentiate thesis titled "*Tempering of press hardening steels PHS1500 and PHS2000: characterization and influence on fracture toughness*" and have been further refined and expanded to reflect the broader scope of the present work.

2.1 Advanced high-strength steels and processing

2.1.1 Press hardening process

Press hardening, also referred to as hot stamping, was patented in 1974 by Norrbottens Jernverk in Luleå [13]. The technology was initially applied in the production of hardened components for agricultural applications, and was subsequently adapted in the 1980s for automotive structural parts [9,14]. The Saab 9000 was among the first passenger vehicles to incorporate press-hardened side-impact beams [15]. Since then, press hardening has evolved into a key manufacturing technology for ultra-high-strength safety components in modern passenger vehicles. Typical applications include A-pillars, B-pillars, bumpers, roof rails, rocker panels, and tunnel reinforcements within the body-in-white structure [16]. The widespread adoption of press-hardened components is driven by their ability to combine high crash resistance with reduced sheet thickness, thereby enhancing passenger safety while contributing to vehicle lightweighting.

Two principal process routes are employed in press hardening: direct and indirect press hardening as illustrated in Figure 1. In direct press hardening, a flat steel blank is heated in a furnace to the austenitization temperature, typically between 900 and 950 °C, and held for several minutes to achieve a fully austenitic microstructure. The blank is then transferred to a press tool, where forming and die quenching are performed in a single step (Figure 1a) [17]. In indirect press hardening, the blank is first cold formed to an intermediate geometry prior to austenitization, followed by reheating and final forming combined with quenching (Fig-

ure 1b). This route can improve dimensional control and surface quality for complex geometries. Compared to conventional cold forming of high-strength steels, press hardening significantly reduces the challenges of excessive springback, cracking, and dimensional inaccuracies. By integrating hot forming with rapid die quenching, thinner sections and more complex geometries can be achieved while maintaining high strength and improved shape accuracy [17,18].

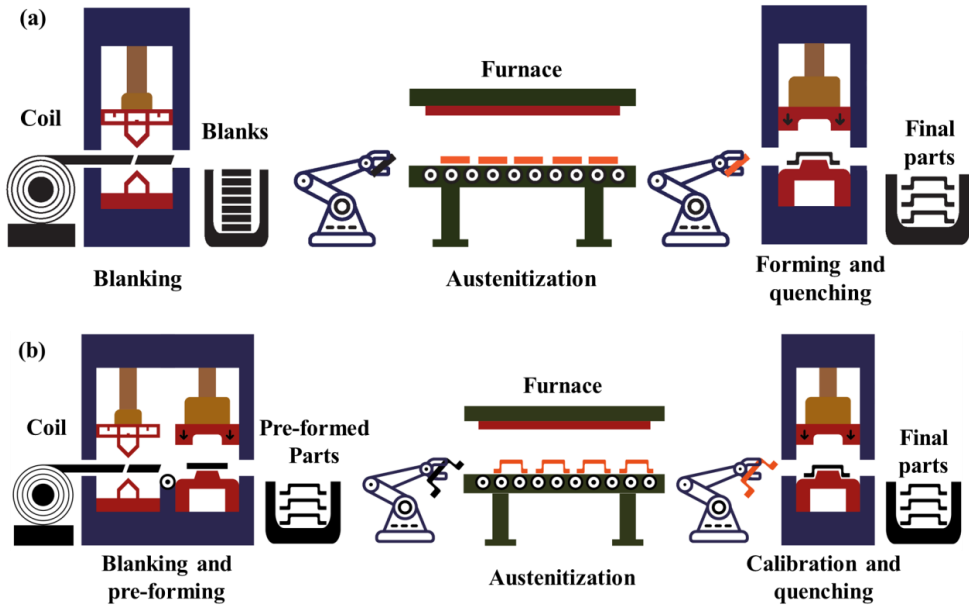


Figure 1: Schematic illustration of press hardening routes: a) direct press hardening, and b) indirect press hardening. Recreated from [4].

In early implementations of press hardening, steel blanks were often heated in furnaces with atmospheres that were not fully controlled, which could result in surface oxidation and decarburization, particularly for uncoated steels. Such surface reactions may adversely affect surface quality and, in severe cases, alter local mechanical properties. To address these challenges, modern press-hardening processes increasingly employ controlled furnace atmospheres and protective coatings, such as Al-Si or Zn-based coatings, which limit the oxidation and decarburization during heating. These advancements have significantly improved process robustness and reduced the need for post-processing treatments [9,14].

The press hardening process is fundamentally governed by phase transformations occurring during heating and subsequent cooling. In the as-delivered condition, press-hardening steels typically exhibit a ferritic-pearlitic microstructure. Upon heating to the austenitization temperature, this microstructure transforms into austenite. During transfer to the forming tool and subsequent die quenching, rapid cooling promotes the transformation of austenite predominantly into martensite, provided that diffusional transformations are sufficiently suppressed. The ability to achieve a fully martensitic microstructure throughout the component thickness is therefore closely linked to the hardenability of the steel and the applied cooling conditions.

Following assembly of press-hardened components into the vehicle body structure, a paint-curing cycle is applied to the body-in-white. During this process, components are typically exposed to temperatures in the range of approximately 140-200 °C for 20-90 minutes [19]. For martensitic press-hardened steels, this thermal exposure may be regarded as a low-temperature tempering treatment. As a consequence, the final mechanical properties of the components can be modified during paint baking [20]. In general, an increase in yield strength and a corresponding reduction in ultimate tensile strength are observed, reflecting the combined effects of strain aging, carbon redistribution, and partial tempering of martensite [21]. Despite these changes, the overall martensitic microstructure remains largely preserved under typical paint-curing conditions.

2.1.2 Metallurgical aspects of press hardening steels

During the press hardening process, several phase transformations take place that govern the final microstructure and mechanical performance of the steel. In the as-delivered condition, press-hardening steels typically exhibit a ferritic-pearlitic microstructure. During the initial heating step, this microstructure transforms into austenite. Subsequent cooling during forming and die quenching leads to the transformation of austenite primarily into martensite under sufficiently high cooling rates, while slower cooling conditions may result in the formation of bainite or ferrite. The press hardening process is designed to produce an ultra-high-strength steel component, with the martensitic transformation playing a central role. In addition to phase transformations, factors such as hardenability, mechanical behaviour, and post-forming treatments like bake hardening are critical for

understanding the performance of press-hardened steels. The following sections therefore summarise the key metallurgical aspects relevant to press hardening.

a. Martensite and martensitic transformation

Martensite is generally considered a diffusionless solid-state transformation product formed during the rapid cooling of austenite. During this transformation, the face-centred cubic (FCC) crystal structure of austenite (γ) changes into body-centred cubic (BCC) or body-centred tetragonal (BCT) martensite, commonly denoted as α' . For the transformation to occur, the Gibbs free energy of martensite must be lower than that of austenite ($G^{\alpha'} < G^{\gamma}$), providing the thermodynamic driving force for the transformation [22].

The martensitic transformation is athermal in nature, meaning that the volume fraction of martensite formed depends primarily on the degree of the undercooling below the martensite start temperature (M_s), rather than on time. As the temperature decreases further below M_s , the fraction of martensite increases and approaches a maximum near the martensite finish temperature (M_f). However, the M_f temperature is less distinct compared to M_s , as a certain fraction of austenite may remain untransformed even at very low temperatures, resulting in retained austenite.

The progress of the martensitic transformation from austenite can be described by the Koistinen-Marburger equation (equation 1) [23,24], which relates the martensite volume fraction to the degree of undercooling below M_s .

$$V_{\gamma} = \exp \{-\alpha(M_s - T_q)\} \quad (1)$$

where V_{γ} is the volume fraction of remaining austenite, T_q is the quench temperature below M_s , and α is an empirical material constant.

The martensitic transformation is characterised by the absence of long-range diffusion of substitutional alloying elements, meaning that the chemical composition of the parent austenite is largely retained in the transformed martensite. While the transformation itself is diffusionless, short-range redistribution of carbon may occur, particularly when the M_s temperature is relatively high. Under such conditions, carbon mobility can lead to auto-tempering, involving carbon segregation to defects and/or precipitation of transition carbides within martensite [25].

Depending on the carbon content of the steel, martensite can exhibit different morphologies, commonly categorised as lath martensite, lenticular martensite, or thin plate martensite. In general, steels with carbon contents above approximately 0.6 wt.% tend to form plate-type martensite, whereas steels with carbon contents below this level predominantly form lath martensite. Press hardening steels typically contain carbon in the range of 0.2-0.4 wt.% and therefore fall within the lath martensite regime. Consequently, the following discussion focuses on lath martensite.

The microstructure of lath martensite exhibits a hierarchical configuration consisting of packets, blocks, and sub-blocks, as schematically illustrated in Figure 2. Packets are formed within individual prior austenite grains and contain groups of martensite variants that share a common close-packed plane relationship with the parent austenite. Each packet is subdivided into blocks, which consist of laths with similar crystallographic orientations, and further into sub-blocks [22].

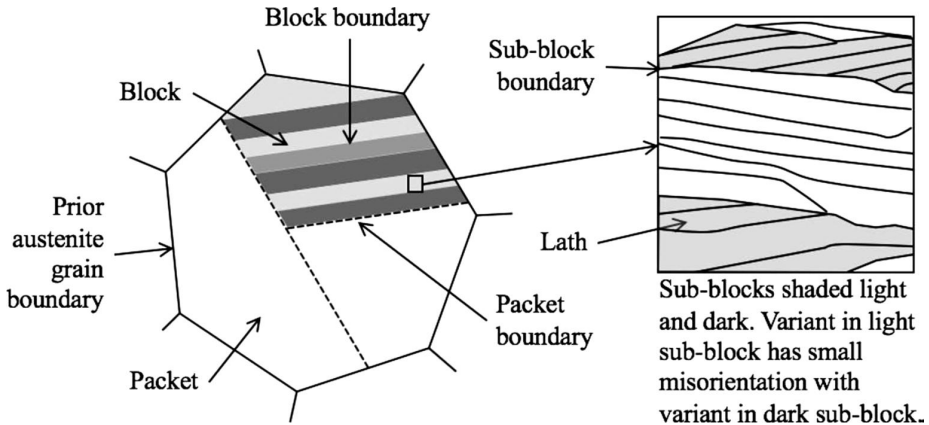


Figure 2: Schematic representation of the morphology of martensitic lath. Adopted from [22].

Tempering is a heat-treatment process applied to martensitic steels to modify their microstructure and mechanical properties, primarily by reducing internal stresses and improving toughness. In press hardening steels, tempering effects are typically associated with relatively low temperatures, either intentionally applied after quenching or occurring unintentionally during processing, such as through auto-tempering [18,21,26].

Martensite is valued for its high strength, however, it is rarely used in the as-quenched condition due to the high internal stresses associated with the martensitic transformation, which can limit ductility of the steel. In low and medium-carbon steels, the tensile strength of as-quenched martensite can exceed 2000 MPa. Low-temperature tempering enhances ductility and toughness with only a minor reduction in strength and hardness. These changes are primarily attributed to the relaxation of internal stresses and the precipitation of fine transition carbides within the martensitic matrix [26–28]. Within the low-temperature tempering range, typically between 150 and 200 °C, carbon supersaturation in martensite is partially relieved through the formation of nanoscale ϵ/η transition carbides [25,29,30]. The presence of these finely dispersed carbides impedes dislocation motion, thereby sustaining high flow stresses, while partial annihilation and rearrangement of dislocations contribute to a minor improvement in total elongation [26,31].

Tempering at temperatures above the low-temperature tempering regime leads to more pronounced microstructural and mechanical changes in martensitic steels. In the tempering range of approximately 200–360 °C, processes such as the decomposition of retained austenite and the transformation of transition carbides into cementite (Fe_3C) become significant [32,33]. Low and medium-carbon steels may retain a smaller fraction of austenite after quenching, which can transform into cementite during subsequent tempering at elevated temperatures (Figure 3). This transformation is generally associated with a detrimental effect on the toughness and ductility of the steel, ultimately leading to brittleness, a phenomenon known as tempered martensite embrittlement [25,34]. Tempering promotes coarsening within the martensitic structure, characterised by the elimination of low-angle boundaries between martensitic laths and the diffusion of carbon from the martensitic matrix into carbide precipitates, subsequently leading to reduced strength and hardness of the steel [27,35].

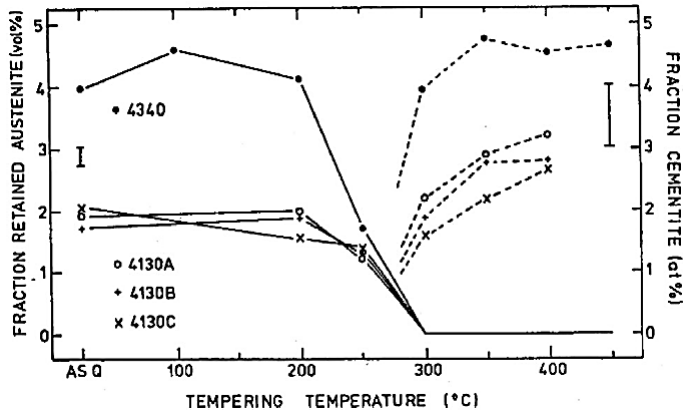


Figure 3: Phase fractions of retained austenite (solid lines) and cementite (dashed lines) during tempering in 4130 and 4340 steels. Adopted from [36].

In addition to tailoring the strength-ductility balance, tempering has been reported to improve the resistance of martensitic steels to hydrogen embrittlement, which represents a critical limitation for the application of ultra-high-strength steels [37,38]. Hydrogen may be introduced during processing or absorbed from service environments, and its presence in martensitic microstructures can lead to premature failure when critical concentrations are reached. Compared to as-quenched martensite, tempered martensite generally exhibits a lower susceptibility to hydrogen embrittlement [39,40]. This behaviour is commonly attributed to the reduction of diffusible hydrogen through tempering, as well as to microstructural changes such as stress relaxation and carbide precipitation that reduce hydrogen mobility [41]. Low-temperature tempering facilitates the release of diffusible hydrogen from the martensitic matrix, thereby decreasing the overall hydrogen content and mitigating embrittlement effects [42,43].

Although the microstructure and properties of martensite can be tailored through tempering, the successful production of ultra-high strength press hardened components first requires sufficient hardenability to ensure martensitic transformation throughout the component during die quenching.

b. Hardenability

Hardenability, which should be distinguished from hardness, refers to the ability of a steel to form martensite to a given depth under specified cooling conditions

[44]. It is fundamentally related to the kinetics of phase transformation and is commonly described in terms of the position of transformation curves in time-temperature-transformation (TTT) or continuous cooling transformation (CCT) diagrams. Increased hardenability corresponds to a shift of diffusional transformation curves toward longer times, thereby delaying the formation of ferrite, pearlite, or bainite and promoting martensitic transformation during cooling.

From a production perspective, high hardenability is advantageous because it enables the formation of a predominantly martensitic microstructure throughout thicker sections of a component without requiring excessively high cooling rates. The hardenability of a steel is primarily influenced by its carbon content, alloying elements, and prior austenite grain size [45].

The formation of martensite during cooling is governed not only by thermodynamic driving force but also by transformation kinetics. In practical processing conditions, the cooling rate determines whether austenite transforms into diffusional products such as ferrite and bainite or into martensite. CCT diagrams provide a graphical representation of these competing transformation paths at different constant cooling rates. An example of CCT diagrams of PHS1500 and PHS2000 press hardening steels estimated using JMatPro is shown in Figure 4. If the cooling curve intersects with the ferrite or bainite regions of the CCT diagram, diffusional transformations occur. Conversely, if the cooling rate is sufficiently high to avoid these regions and reach the M_s temperature without prior transformation, a predominantly martensitic microstructure can be obtained.

In press-hardening processes, rapid die quenching is employed to achieve cooling rates high enough to suppress diffusional transformations and promote full martensitic transformation throughout the component thickness. The minimum cooling rate required to obtain a fully martensitic microstructure is often referred to as the critical cooling rate and depends on the hardenability of the steel [18]. Steels with higher hardenability require lower critical cooling rates, thereby increasing processing robustness and enabling uniform properties even in thicker sections.

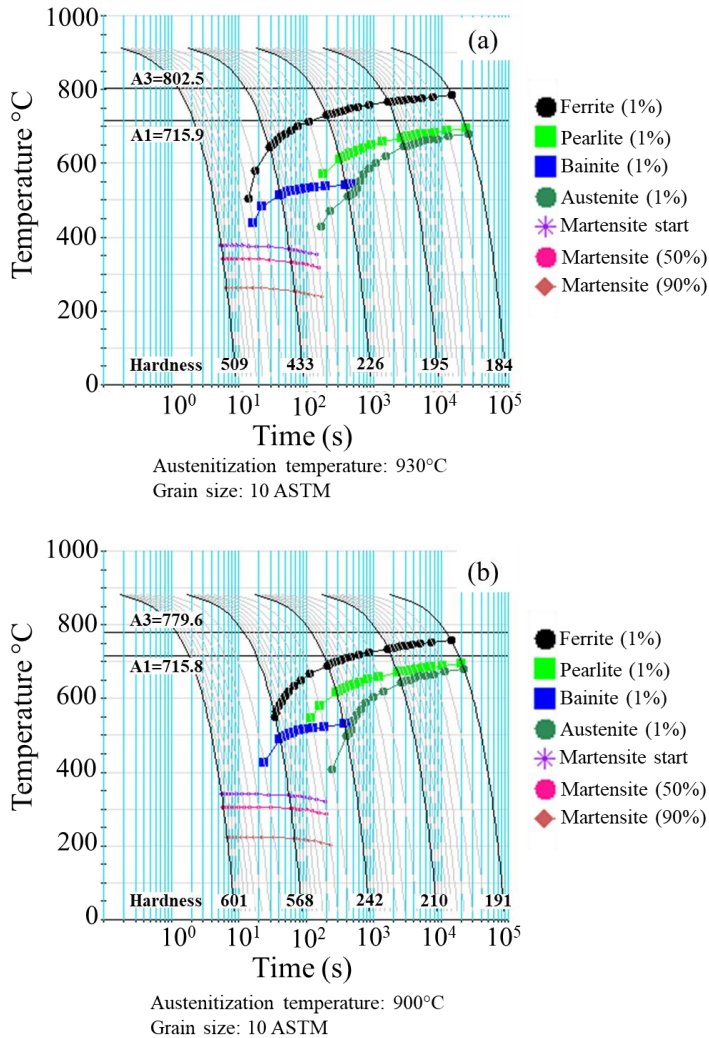


Figure 4: CCT diagrams as estimated using JMatPro software for (a) PHS1500 and (b) PHS2000.

Hardenability depends not only on the nominal carbon content of the steel, but more specifically on the amount of carbon dissolved in austenite during austenitization [44]. Only carbon in solid solution contributes effectively to transformation behaviour. Increasing carbon content lowers the M_s temperature and stabilises austenite, while simultaneously retarding diffusional transformations such as ferrite and pearlite formation. As a result, steels with higher carbon content generally

exhibit improved hardenability. Alloying elements such as manganese, chromium, and molybdenum further enhance hardenability by delaying diffusional phase transformations [46].

Press-hardening steels achieve high hardenability through minor additions of boron, typically in the range of 30-50 ppm [9]. Such small additions can provide a hardenability increase comparable to substantially larger additions of substitutional alloying elements. Boron enhances hardenability primarily through segregation to prior austenite grain boundaries, where it suppresses ferrite nucleation and thereby delays diffusional transformations [47,48]. To ensure the effectiveness of boron, small additions of titanium are commonly introduced to bind residual nitrogen in the form of stable TiN precipitates [20]. This prevents the formation of boron nitrides, which would otherwise reduce the amount of boron available in solid solution and diminish its beneficial effect on hardenability [49].

c. Microstructure-property relationships

The exceptional strength of martensite in low- and medium-carbon steels originates from the unique microstructure features introduced by the diffusionless martensitic transformation. The as-quenched martensitic microstructure is characterised by an ultrafine lath morphology, very high dislocation density, and supersaturation of carbon in the lattice. These features act synergistically to produce the exceptionally high strength and hardness associated with martensite [50,51].

The martensite transformation proceeds by shear without long-range diffusion, resulting in the formation of a thin lath structure. The refinement of lath size is a consequence of strain accommodation requirements during transformation: as individual martensite laths form, the surrounding austenite hardens, limiting further thickening and promoting the nucleation of additional laths [30]. This process produces a microstructure with a high interfacial area per unit volume. From a mechanical perspective, the lath thickness and hierarchical packet/block arrangement constitute the effective grain size of martensite [35]. Even after substantial tempering, when dislocation density is reduced, the retained fine lath morphology continues to act as a primary strengthening feature.

The high dislocation density, reported to approach 10^{16} m^{-2} in as-quenched martensite, originates from crystallographic accommodation associated with the

change from the close-packed austenite to the more open martensite lattice [52,53]. The resulting dense dislocation network is a major contributor to the flow stress, leading to the high hardness and tensile strength of martensite. Carbon plays a critical role in the mechanical behaviour of martensite [54–56]. Because the transformation is diffusionless, carbon atoms dissolved in austenite become trapped in interstitial sites within the martensite lattice, producing supersaturation and, in higher carbon steels, measurable tetragonality [57,58]. The associated lattice distortion contributes to solid solution strengthening. In addition, a significant fraction of carbon segregates to dislocations and lath boundaries during quenching, particularly in low-carbon steels [25]. This segregation stabilises the dislocation structure, enhances pinning, and increases resistance to dislocation motion. The interaction between carbon and dislocations therefore reinforces the already high strength associated with the dislocation network.

Upon low-temperature tempering, transition carbides precipitate within the laths as very fine particles on the order of a few nanometres [59]. These nanoscale precipitates introduce additional barriers to dislocation motion, while the dislocation density remains relatively high. The combined effect of fine carbide dispersion and residual dislocation substructure produces ultrahigh strength and substantial strain hardening capacity in low-temperature tempered martensite. As tempering temperature increases further, transition carbides are replaced by coarser cementite, and recovery reduces dislocation density, leading to softening [27].

In an integrated sense, the mechanical strength of martensite emerges from the synergistic interaction of the fine lath morphology, extremely high dislocation density, carbon supersaturation and segregation, and nanoscale carbide precipitation. The martensitic transformation establishes a highly strained, hierarchical microstructure in which carbon and dislocations are coupled. Subsequent tempering modifies, but does not eliminate, the structural framework established during transformation [27,60]. Consequently, the mechanical behaviour of martensite reflects the evolving balance between dislocation strengthening, precipitation strengthening, and lath-scale structural refinement.

d. Bake hardening

Bake hardening (BH) refers to the increase in yield strength that occurs when a plastically deformed steel is subjected to a subsequent low-temperature heat treatment [61]. In automotive manufacturing, this strengthening typically takes place during the paint-baking cycle, where formed body components are exposed to temperatures in the range of approximately 150-200 °C for paint curing [20]. In conventional bake-hardenable steels, the increase in yield strength arises primarily from the interaction between interstitial solute carbon atoms and dislocations introduced during prior forming operations [62]. A key advantage of bake hardening is that no additional processing steps are required, as the strengthening effect occurs during the standard paint-curing operation already integrated into the production route.

Fundamentally, bake hardening can be described as a manifestation of static strain ageing (SSA), in which interstitial carbon atoms play a central role [62]. During ageing, carbon diffuses toward the elastic stress fields surrounding dislocations introduced by prior deformation, leading to the formation of so-called Cottrell atmospheres that effectively pin dislocation motion [63,64]. With increasing ageing time and temperature, successive clustering of carbon atoms may occur, potentially followed by the precipitation of fine transition carbides [62,65]. The relative contribution of these mechanisms depends on the carbon content and thermal conditions. The resulting bake hardening response is influenced by several factors, including the concentration of solute carbon, dislocation density (i.e., pre-strain level), grain size, and processing parameters such as cooling rate and annealing conditions [61].

In martensitic steels, the bake hardening response is more complex than in predominantly ferritic bake-hardenable steels. Unlike ferritic steels, as-quenched martensitic microstructures contain a very high density of dislocations generated during the athermal martensitic transformation, even in the absence of externally applied deformation [66]. As a result, martensitic steels may exhibit a measurable strengthening response during baking even without prior deformation.

The bake hardening behaviour of martensitic steels is further complicated by the auto-tempering phenomenon and the microstructural heterogeneities established

during quenching. Owing to the athermal nature of martensitic transformation, newly formed martensite is characterised by a high dislocation density, refined lath morphology, and significant internal stresses [25]. These features provide abundant sites for rapid carbon redistribution. Carbon atoms can segregate to dislocations and lath boundaries, forming Cottrell atmospheres already during quenching [67]. Simultaneously, precipitation of transition carbides may occur, reducing the amount of carbon remaining in solid solution.

Consequently, the solute carbon available for subsequent strengthening during paint baking is governed by the dynamic balance between segregation and carbide precipitation established during quenching [68,69]. During the paint-curing cycle, which, for martensitic steels, effectively corresponds to a low-temperature tempering treatment, two competing mechanisms dominate: (i) further precipitation of fine iron carbides, contributing to precipitation strengthening, and (ii) recovery and relaxation of the martensitic matrix, leading to a reduction in internal stresses and dislocation density [21,31,69]. The observed bake hardening response therefore reflects the interplay between strengthening and softening processes.

2.1.3 Quenching and partitioning

Quenching and partitioning (Q&P) is a heat-treatment strategy developed to stabilise retained austenite in advanced high-strength steels, thereby enhancing strength-ductility balance. Originally proposed by Speer et al. [70–72], the Q&P process involves full or partial austenitization followed by rapid cooling to a temperature between the martensite start (M_s) and martensite finish (M_f) temperatures. This interrupted quench produces a controlled fraction of supersaturated martensite while retaining untransformed austenite. Subsequently, the steel is held either at the quenching temperature (one-step Q&P) or reheated to a temperature above M_s (two-step Q&P) to enable carbon partitioning from the supersaturated martensite into the remaining austenite. A schematic illustration of the Q&P process is shown in Figure 5. The enrichment of austenite in carbon enhances its stability against further transformation during final cooling to room temperature.

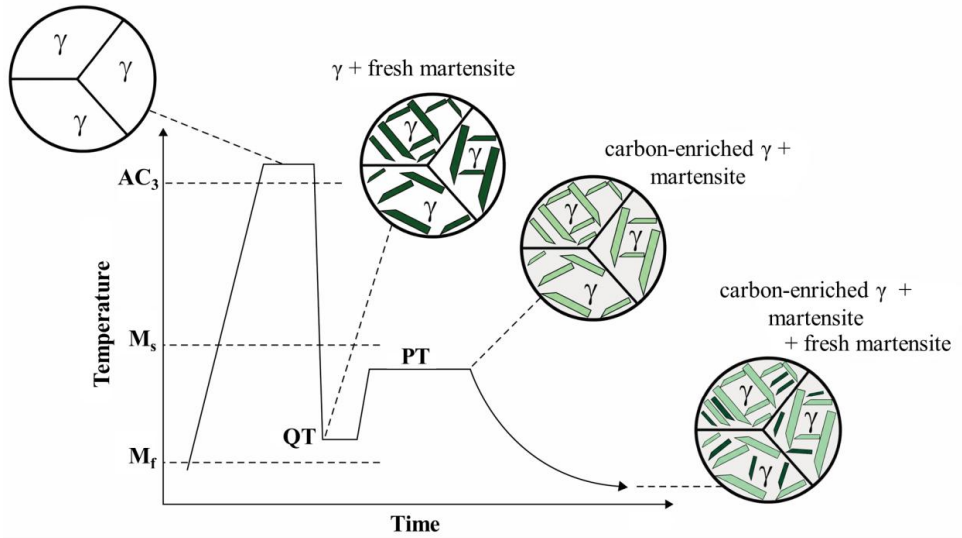


Figure 5: Schematic illustration of the two-step Q&P with corresponding microstructure, where QT and PT indicate quenching and partitioning temperatures, respectively. Adopted from [73].

The Q&P concept has also been explored in combination with press hardening as a potential route to achieve an improved balance between strength and ductility in ultra-high-strength components [74–78]. A schematic representation of the press hardening route with integrated Q&P processing is provided in Figure 6. By integrating controlled quenching and carbon partitioning steps into the press-hardening cycle, a multiphase microstructure containing martensite, carbide-free bainite, and stabilised retained austenite may be obtained. Despite the promising mechanical performance reported in laboratory-scale studies, industrial implementation within conventional press-hardening lines remains challenging. The partitioning stage requires precise thermal control and sufficient time to allow carbon redistribution and austenite stabilisation, which may conflict with the short cycle times and rapid cooling conditions typical of industrial press hardening.

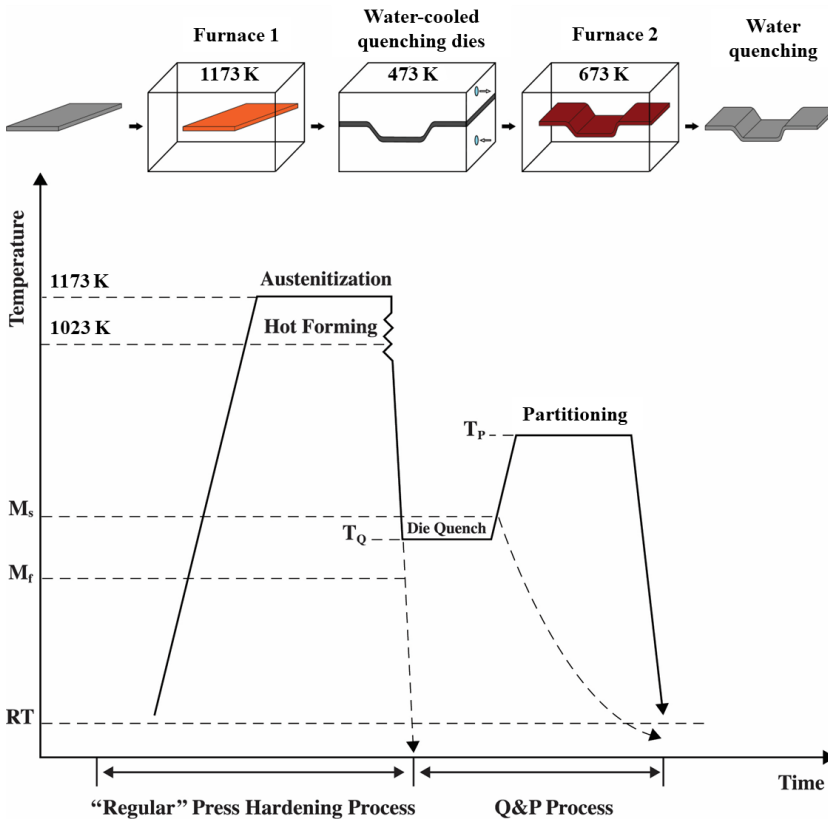


Figure 6: Schematic of the modified press hardening process integrated with quenching and partitioning. Adopted from [74].

Carbon partitioning from supersaturated martensite to austenite during the partitioning stage is central to stabilising retained austenite at room temperature. Successful carbon enrichment requires suppression of competing reactions, particularly carbide precipitation within martensite. To promote carbon partitioning, alloying elements such as silicon and aluminium are commonly employed, as they retard cementite formation and thereby facilitate carbon retention in austenite [79,80]. The resulting fraction and stability of retained austenite significantly influence the mechanical response. Stabilised austenite can transform under applied stress, contributing to enhanced strain hardening and an improved strength-ductility balance through the transformation-induced plasticity (TRIP) effect [81–83].

The partitioning stage, typically lasting several minutes, is a critical step in the Q&P process. The selected partitioning temperature and holding time strongly influence the efficiency of carbon redistribution and, consequently, the stability and volume fraction of retained austenite [84]. In addition, the quenching temperature determines the initial fraction of martensite formed prior to partitioning [85], thereby governing the available carbon reservoir and the subsequent partitioning kinetics.

A detailed understanding of carbon redistribution during Q&P is therefore essential for elucidating transformation mechanisms and optimising processing parameters. However, tracking carbon diffusion and phase evolution in real time remains challenging when relying on conventional laboratory X-ray diffraction techniques. In contrast, in-situ high-energy X-ray diffraction provides enhanced temporal and phase-resolution capabilities, enabling direct observation of phase transformations and carbon redistribution during thermal treatments, as demonstrated in recent studies [85–91].

Accelerating transformation kinetics is advantageous in Q&P processing, as reduced holding times improve industrial feasibility and productivity. In this context, isothermal holding within the bainitic temperature range, in the presence of pre-existing martensite, has been proposed as a means of promoting carbide-free bainite formation [92–94]. During bainitic transformation, carbon is rejected from the bainitic ferrite into the surrounding austenite, contributing to its enrichment and stabilisation. Consequently, carbon partitioning to austenite may occur not only from supersaturated martensite but also from the formation of bainite [86,95]. The relative contribution of these mechanisms depends on the initial microstructural state, particularly on the fraction of martensite formed during the initial quench. When the quench-stop temperature is low, and the microstructure contains a high fraction of martensite, carbon enrichment is predominantly governed by martensite-to-austenite partitioning. In contrast, for higher quench-stop temperatures closer to M_s , carbon enrichment results from a combination of partitioning from martensite and carbon rejected during bainitic transformation [85].

2.2 Phase transformation during thermomechanical processes

During press hardening, steel blanks are formed at elevated temperatures and subsequently quenched to obtain a predominantly martensitic microstructure. The final strength of the component depends largely on the hardenability of the steel and the cooling conditions during die quenching. However, the forming stage itself may influence phase transformation behaviour. This thermomechanical history significantly alters transformation kinetics, phase distribution, and final mechanical properties [11]. A large body of literature demonstrates that prior austenite deformation primarily accelerates diffusive transformations, while generally suppressing martensitic transformation, although the overall response depends on deformation conditions such as temperature, strain, and strain rate [96–102].

Deformation of austenite markedly accelerates ferrite transformation. This phenomenon is often described as deformation-induced ferrite transformation (DIFT), in which ferrite forms during deformation rather than solely during cooling [103,104]. Min et al. [97] showed that deformation significantly shortens the incubation time for ferrite formation and can even shift the transformation mechanism from growth-controlled to nucleation-controlled. Similarly, Zhou et al. [105] observed that deformation shifts the ferrite region in the continuous cooling transformation diagram toward shorter times, indicating faster kinetics.

The underlying mechanisms responsible for this acceleration are well established. First, plastic deformation increases the dislocation density within austenite, which provides abundant heterogeneous nucleation sites. Second, deformation introduces stored strain energy, which increases the thermodynamic driving force for the austenite-to-ferrite transformation. This increase in free energy of the deformed austenite enhances the transformation driving force (ΔG) and reduces the critical nucleation barrier. As a result, ferrite nucleation occurs earlier and more rapidly, leading to a significant reduction in incubation time [97,103,104].

In contrast to ferrite, martensitic transformation is generally suppressed by prior austenite deformation. This suppression is primarily attributed to mechanical stabilisation of austenite, whereby deformation-induced dislocations increase the

strength of austenite and hinder the movement of martensitic transformation interfaces [98]. As a result, greater undercooling is required to initiate martensite formation, leading to a reduction in M_s temperature and a decrease in martensite fraction [11,106]. Additionally, the accelerated formation of ferrite and bainite consumes austenite and enriches the remaining austenite in carbon, further stabilising it and suppressing martensitic transformation. This effect is clearly demonstrated in dilatometric studies, where deformation leads to reduced martensitic dilatation due to the prior formation of diffusive phases (Figure 7) [11,98].

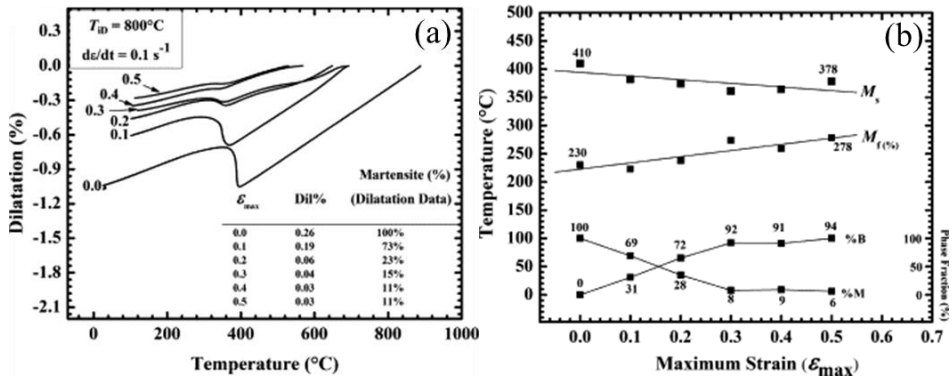


Figure 7: Effect of strain on phase transformation deformed at 800 C. (a) dilatation vs temperature curves; values near the curves indicate the amount of strain applied. (b) evolution of M_s and M_f temperatures and corresponding phase fractions.

Adopted from [11].

2.2.1 Effect of deformation parameters

The influence of prior austenite deformation on phase transformation is strongly dependent on deformation parameters, particularly temperature, strain, and strain rate. These parameters control the evolution of dislocation density, stored deformation energy, and the available time for diffusion, thereby determining the balance between diffusive and martensitic transformations.

Among these parameters, deformation temperature plays a dominant role. Deformation at lower temperatures generally promotes ferrite and bainite formation, as recovery and recrystallisation processes are limited, leading to higher retained dislocation density and stored energy. In contrast, deformation at higher temperatures

facilitates dynamic recovery and recrystallisation, which reduces dislocation density and stored energy. As a result, the acceleration of diffusive transformations is weakened, and a larger fraction of martensite can be obtained during subsequent cooling [97,100,107].

Increasing strain leads to a higher dislocation density and greater stored deformation energy, which strongly promotes ferrite formation. At sufficiently high strain levels, ferrite can become the dominant phase, significantly reducing the fraction of martensite after cooling [12,108]. The role of strain rate is more complex due to competing effects [11]. On one hand, higher strain rates increase dislocation density, which would enhance the driving force for diffusive transformations [12]. On the other hand, higher strain rates reduce the time available for diffusion during deformation, which can suppress ferrite formation [97]. As a result, the influence of strain rate on phase transformation is often non-monotonic.

In addition to individual parameters, the interaction between deformation and cooling conditions is critical. Deformation effectively reduces the hardenability of the material by accelerating diffusive transformations, thereby increasing the critical cooling rate required to achieve a fully martensitic microstructure. Consequently, cooling rates that are sufficient for undeformed austenite may no longer prevent ferrite or bainite formation after deformation [11,12,97]. This interaction highlights the importance of considering both deformation history and thermal conditions when designing hot stamping processes.

2.3 Fracture toughness

Fracture toughness is a key mechanical property describing a material's resistance to crack initiation and propagation. It is an essential parameter in the design of structural components where sudden fracture must be avoided. In the automotive industry, fracture toughness has gained increasing attention with the growing use of ultra-high-strength steels, which, despite their high load-bearing capacity, may exhibit reduced resistance to crack initiation and propagation at elevated strength levels. Consequently, fracture toughness plays an important role in assessing the crash performance of press-hardened components used in modern vehicle struc-

tures [109,110]. The increasing interest in this property has led to extensive research aimed at understanding fracture behaviour in ultra-high-strength steels [111–113].

Fracture mechanics provides the theoretical framework for understanding and quantifying material failure associated with crack initiation and propagation. The foundations of fracture mechanics were established by Griffith, who demonstrated that the fracture strength of brittle materials is strongly influenced by the presence of flaws or discontinuities [114]. His work revealed that the measured fracture stress of glass specimens was significantly lower than the theoretical strength, leading to the conclusion that crack-like defects control fracture behaviour and introduce a pronounced size effect. This concept formed the basis of linear elastic fracture mechanics (LEFM), which describes crack propagation in materials where plastic deformation at the crack tip is limited. For materials exhibiting significant plastic deformation prior to fracture, LEFM is no longer sufficient. To address such cases, Rice [115] extended the theoretical framework to account for elastic-plastic behaviour, leading to the development of elastic-plastic fracture mechanics (EPFM).

2.3.1 Linear elastic fracture mechanics

LEFM describes crack behaviour in materials where plastic deformation at the crack tip is limited, and the surrounding material response can be approximated as linear elastic. The central objective of LEFM is to quantify the severity of the stress field in the vicinity of a crack. This is achieved through the stress intensity factor K . For a crack subjected to remote loading, the stress intensity factor can be expressed as:

$$K = Y\sigma\sqrt{\pi a} \quad (2)$$

where Y is a geometry-dependent correction factor, σ is the applied stress, and a represents a characteristic crack dimension. When the stress intensity factor reaches a critical value, crack propagation becomes unstable. This critical value is defined as the fracture toughness of the material under linear elastic conditions.

Within the framework of LEFM, the critical stress intensity factor is commonly denoted as K_C . The measured value of K_C depends on the thickness of the specimen because the stress state at the crack tip changes from plane stress in thin sections to plane strain in thicker sections. With increasing specimen thickness, the apparent fracture toughness decreases until it reaches a constant minimum value that becomes independent of further increases in thickness. This limiting value is known as the plane strain fracture toughness, K_{IC} , and is considered an intrinsic property for a given material under linear elastic fracture conditions.

2.3.2 Elastic-plastic fracture mechanics

Many engineering materials exhibit significant plastic deformation prior to fracture. Under such conditions, the assumptions of LEFM are no longer valid, as the plastic zone that develops at the crack tip cannot be considered negligible. To account for this behaviour, fracture mechanics concepts were extended to incorporate elastic-plastic material response, leading to the development of elastic-plastic fracture mechanics (EPFM).

The J-integral is a key parameter in elastic-plastic fracture mechanics used to characterise the crack-driving force in materials undergoing both elastic and plastic deformation. Introduced by Rice [115], the J-integral represents the energy release rate associated with crack extension under conditions where significant plastic deformation develops near the crack tip. A fundamental property of the J-integral is its path independence, meaning that it can be evaluated along any arbitrary contour surrounding the crack tip provided that the stress and strain fields are known. The mathematical form of the J-integral is given by Equation (3):

$$J = \int_C \left(W dy - T_i \frac{\partial u_i}{\partial x} ds \right) \quad (3)$$

Where W is the strain energy density, C denotes an arbitrary contour surrounding the crack tip (Figure 8), T_i represents the components of the traction vector acting on the contour, and u_i is the displacement vector. The coordinates x and y define a Cartesian system with the x -direction normal to the crack front, while ds represents an increment of the contour C .

The strain energy density is defined according to the following equation (4):

$$W = \int \sigma_{ij} d\varepsilon_{ij} \quad (4)$$

where σ_{ij} and ε_{ij} denote the stress and strain components, respectively.

Under monotonic loading, crack initiation occurs when the J-integral reaches a critical value, denoted as J_C , which represents the fracture resistance of the material under elastic-plastic conditions. This parameter is analogous to the critical stress intensity factor K_{IC} in linear elastic fracture mechanics. The critical J-integral value corresponds to the onset of stable crack propagation and provides a measure of the fracture toughness of ductile materials.

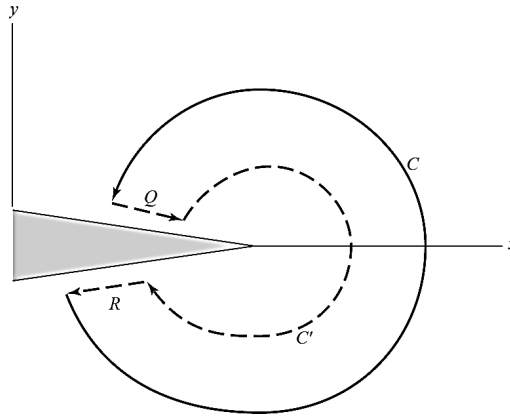


Figure 8: Arbitrary line contour surrounding the tip of a crack [116].

2.4 Modelling austenite grain growth

The evolution of the parent austenite grain size (PAGS) is of central importance, as it influences subsequent phase transformation kinetics and thereby indirectly affects the mechanical response of the final microstructure. In order to enable predictive process simulations, a constitutive description of austenite grain growth as a function of thermal history is required.

The modelling approach adopted is based on classical curvature-driven grain boundary migration, where grain growth is driven by the reduction of total grain

boundary energy. The evolution of the parent austenite grain size can be described using the grain growth formulation as expressed by equation (5) [117]:

$$\frac{d\bar{D}}{dt} = k \frac{1}{\bar{D}} \quad (5)$$

where \bar{D} denotes the mean grain diameter and k is a temperature-dependent coefficient and t is the time. This expression reflects the curvature-driven nature of grain growth, where the growth rate decreases with increasing grain size. Integration of this equation leads to a power-law relationship between grain size and time. In general, grain growth can be expressed as in equation (6):

$$\bar{D}^n - \bar{D}_0^n = kt \quad (6)$$

where \bar{D}_0 is the grain diameter at the onset of growth, and n is the grain growth exponent. Differentiation of the generalised expression with respect to time yields the corresponding rate form:

$$\frac{d\bar{D}}{dt} = \frac{k}{n(\bar{D})^{n-1}} \quad (7)$$

To account for temperature dependence, the kinetic constant k is expressed using an Arrhenius-type relationship as expressed by equation (8):

$$k = k_0 \exp\left(-\frac{Q}{RT}\right) \quad (8)$$

where k_0 is a pre-exponential constant, Q the activation energy for grain boundary migration, R the ideal gas constant, and T the absolute temperature in Kelvin (K). Substitution of this expression into the rate equation gives:

$$\frac{d\bar{D}}{dt} = k_0 \exp\left(-\frac{Q}{RT}\right) \frac{1}{n(\bar{D})^{n-1}} \quad (9)$$

The measured thermal histories were discretised using a time increment of 1 s, and the rate equation was integrated using a forward Euler scheme, enabling prediction of grain growth under both isothermal and non-isothermal austenitization conditions.

The model parameters k_0 , Q , n , and the initial grain size \bar{D}_0 are identified from isothermal grain growth experiments. The formulation assumes homogeneous growth governed by curvature-driven boundary migration and constant effective

pinning conditions. At higher austenitization temperatures, where abnormal grain growth and local variations in pinning may occur, deviations from model predictions can arise, reflecting the limitations of mean-field grain size descriptions.

Chapter 3 Materials and Methods

3.1 Materials

The materials investigated in the present work were composed of three advanced high-strength steels (AHSS), two of which are intended for press hardening applications and the third is a quenching and partitioning (Q&P) steel grade. The press-hardened steel grades used are commercially available and uncoated, with nominal strength levels of 1.5 GPa and 2.0 GPa, referred to as PHS1500 and PHS2000, respectively. The Q&P steel is a low-carbon, high-Si-containing steel, referred to as Q&P. The chemical composition ranges for the steels are displayed in Table 1. Detailed chemical compositions for each steel are provided in the appended papers. Table 2 shows the sheet thicknesses and indicates the research studies in which they were investigated.

Table 1: Chemical composition ranges in wt.% as provided by the material supplier for the three steels [118,119].

Material	C	Si	Mn	P	S	Cr	B	Nb+Ti
PHS1500	0.20-0.25	0.15-0.35	1.00-1.35	0.025	0.005	0.35	0.0020-0.0050	-
PHS2000	0.30-0.38	0.15-0.35	1.10-1.50	0.025	0.005	0.35	0.0010-0.0050	0.2
Q&P	0.20	1.50	2.00	-	-	0.50	-	-

**P, S, Cr and Nb+Ti are shown with max composition values.*

Table 2: Sheet thickness of steels and corresponding papers.

Material	Thickness (mm)	Paper
PHS1500	2.5	Paper I, Paper II, and Paper IV
PHS2000	2.5 & 3	Paper I, Paper II, and Paper III
Q&P	10	Paper V

3.2 Processes

In this work, different heat treatment processes were performed, including quenching and tempering, press hardening, bake hardening, and quenching and partitioning. A summary of each process is provided below.

3.2.1 Quenching and tempering

The Q&T process was employed in *Paper I*. During the Q&T process, the steels were first fully austenitized in a muffle furnace and then quenched in oil at room temperature. Subsequently, the steels were tempered in a salt bath furnace at different tempering temperatures and durations, followed by air cooling to room temperature. The heat treatment conditions are schematically shown in Figure 9.

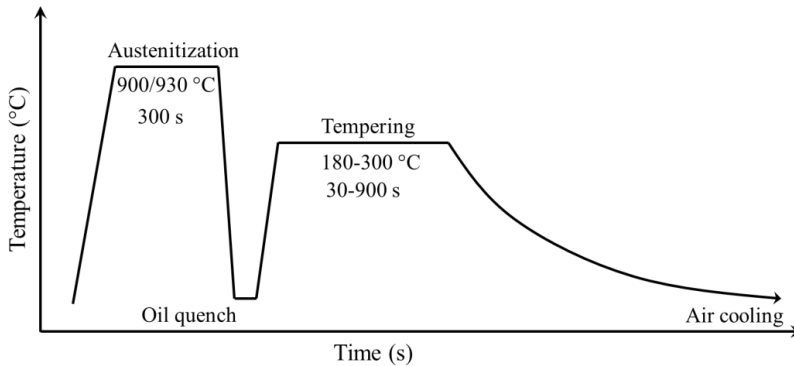


Figure 9: Schematic illustration of the quenching and tempering process.

3.2.2 Press hardening

Lab-scale press hardening experiments (*Paper I*), without deformation, were carried out using a flat tool mounted in a tensile testing machine. The samples were first austenitized then transferred to the press where they were die quenched using a constant contact pressure of 5 MPa. The pressure time was varied, allowing the samples to cool down to different quenching temperatures (100 °C, 150 °C, 200 °C, and 300 °C). Thereafter, the samples were allowed to cool down to room temperature in air. To ensure temperature control, the samples' temperature was continuously monitored using a K-type thermocouple welded to the thickness face of the specimen. Figure 10 shows a schematic illustration of the lab-scale pressing tool used in this work, and an example of the temperature profile during press hardening after die quenching to 300 °C.

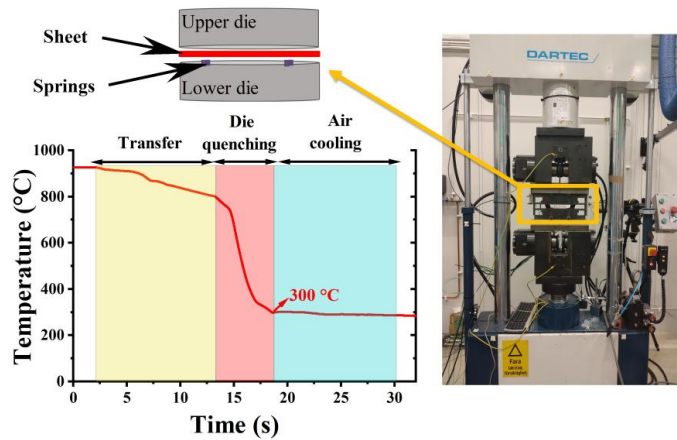


Figure 10: Schematic illustration of the press hardening process.

In Paper II, the press hardening process was carried out at the company Gestamp HardTech (Luleå, Sweden), using a small pilot press hardening line intended for research. This allowed for pressing bigger sheet blanks from which samples could be machined afterwards for mechanical testing. The blanks with a dimension of 240 mm x 240 mm were first austenitized, then transferred to the flat pressing tools and quenched under a constant contact pressure of 5 MPa. The pressure was maintained for about 8 seconds, allowing the blanks to cool below 160 °C at the point of die opening. Finally, the blanks were cooled to room temperature in air.

3.2.3 Bake hardening

In the paper addressing the effect of paint baking treatment (*Paper II*), the samples were subjected to baking treatment in a muffle furnace after the press hardening process. The treatment was conducted at 175 °C for a duration of 20 minutes, followed by air cooling to room temperature.

3.2.4 Quenching and partitioning

The quenching and partitioning process was used for the Q&P steel (*Paper V*). This process was conducted in situ using a DIL 805 A/D dilatometer (TA Instruments, USA). Hollow cylindrical specimens with an outer diameter of 4 mm, a wall thickness of 1 mm, and a height of 10 mm were machined using electrical discharge machining (EDM). After the steel was fully austenitized at 930 °C for 120 s, the samples were quenched to 340 °C at a cooling rate of 100 °C/s followed

by isothermal holding at either 400 °C for 600 s or 450 °C for 180 s. An additional sample was chosen to undergo a one-step quenching and partitioning treatment at 340 °C for 900 s. Temperature control during the treatments was achieved via a Pt/Pt-Rh thermocouple, which was spot-welded to the specimen surface.

In addition to the Q&P process, a bainitizing treatment was conducted on the same steel as follows:

- Two-step austempering: samples were quenched to 370 °C at a cooling rate of 100 °C/s and then austempered at 400 °C or 450 °C for 600 s and 180 s, respectively.
- Single-step austempering: samples were directly quenched at the same cooling rate to the target temperatures of 370 °C, 400 °C, or 450 °C, held isothermally for 900 s, and finally air-cooled to room temperature.

It can be mentioned that the bainitizing process also began with a fully austenitization at 930 °C for 120 s.

3.3 Gleeble simulations

The press hardening is a high temperature forming process in which the component is formed in the austenite region at high temperature prior to quenching. The effect of prior deformation of austenite on the phase transformation was investigated using a Gleeble 3800 thermomechanical simulator (*Paper III*). The tests were carried out on tensile-shaped specimens as illustrated in Figure 11.

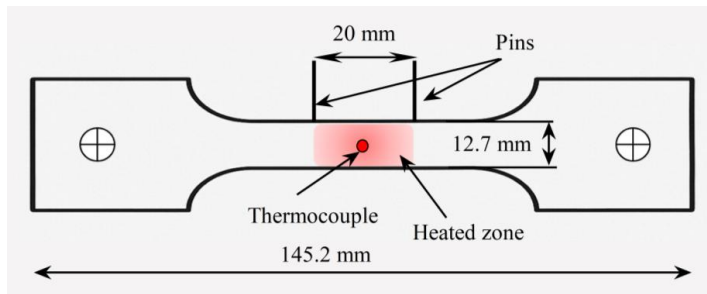


Figure 11: Tensile specimen used for thermomechanical experiments.

The specimens were EDM machined with the rolling direction parallel to the tensile direction. A set of thermomechanical cycles was designed as illustrated in Figure 12. Temperature was monitored during the experiment using a K-type thermocouple, spot-welded to the centre point of each specimen. The process began with heating the specimens to 900 °C at a rate of 10 °C/s and soaking for 60 s. Subsequently, the specimens were cooled to one of three initial deformation temperatures: 820 °C, 760 °C, or 700 °C at a cooling rate of 10 °C/s. Once at the designated deformation temperature, the specimens were held for 1 second before undergoing tensile deformation with varying strokes of 3, 6, and 10 mm, at three strain rates of 0.1, 1, and 10 s⁻¹. Finally, specimens were quenched to room temperature using compressed air.

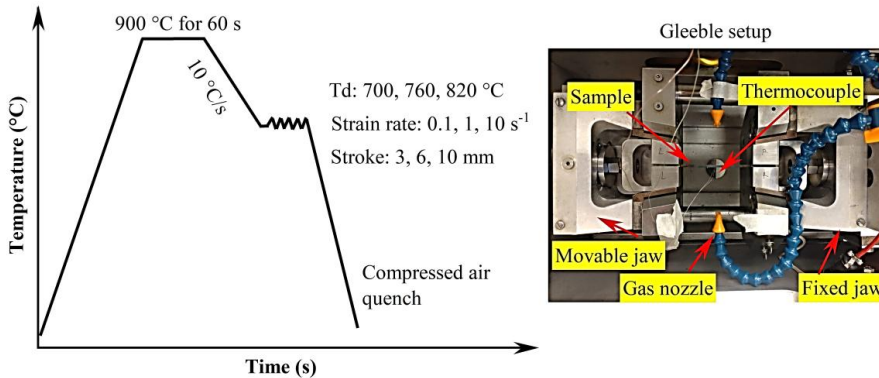


Figure 12: Thermomechanical cycles and the Gleeble setup. T_d indicates the deformation temperature.

The phase transformation during the thermal cycles was monitored by means of an optical dilatometer system, which was used during the Gleeble dilatation tests. Two reference pins were welded onto the specimen edge along the thickness direction, positioned around the midpoint of the gauge length with an initial distance of approximately 20 mm between them, as shown in Figure 11, where the temperature distribution is expected to be uniform. The dilatometer tracked the change in length between the pins, enabling precise measurement of thermal and transformational dilation of the specimen during heating and cooling. The resulting dilatometry curves were used to analyse transformation behaviour, including austenite formation and its subsequent decomposition. Transformation events were

identified based on characteristic changes in the slope of the relative length change vs temperature response.

3.4 Microstructural characterisation

The microstructure was analysed using light optical microscopy (OM), scanning electron microscopy (SEM) and energy backscatter diffraction (EBSD). Prior to analysis, samples underwent metallographic preparation involving grinding and polishing according to conventional metallographic practices. Thereafter, samples were etched with a 3 % Nital solution when necessary. The OM analysis was carried out using a Nikon Eclipse MA200 microscope. SEM investigations were performed using either a high-resolution FEI Magellan 400 or a Jeol JSM-IT300LV microscope. The EBSD technique was employed to determine the prior austenite grain size, utilising a Tescan Amber X2 FIB-SEM. Phase area fractions were quantified using the Trainable Weka Segmentation plugin in Fiji (ImageJ) software [120].

In addition to metallographic analysis, X-ray diffraction (XRD) was performed to determine the dislocation density using a Panalytical Empyrean diffractometer equipped with Cu K α radiation, operated at 40 kV and 45 mA. Data were collected from polished samples on surfaces parallel to the rolling direction over a 2θ range of 35° to 110°, with a step size of 0.01°.

In-situ high energy X-ray diffraction (HEXRD) experiments were carried out at the P07B beamline of Hereon at the PETRA III facility (DESY, Germany) to monitor the phase evolution during quenching, reheating, partitioning, and austempering of the Q&P steel (*Paper V*). The experimental setup, as illustrated in Figure 13, employed a monochromatic X-ray beam with an energy of 87.1 keV ($\lambda = 0.14235 \text{ \AA}$), which enabled transmission-mode operation due to its high penetration power. Instrument calibration was carried out using LaB $_6$ powder (SRM 660C, NIST, USA). Diffraction patterns were collected using a PerkinElmer XRD1621 detector (pixel size: 200 μm), positioned at a distance of 1392 mm from the sample. The resulting 2D Debye–Scherrer rings were converted to conventional intensity vs. 2θ profiles using the Fit2D software. Subsequently, the 1D

diffraction patterns were analysed through Rietveld refinement using Match! software.

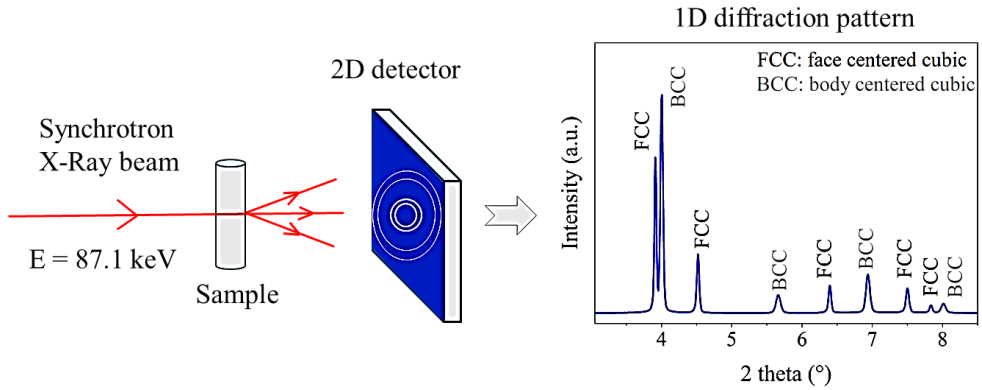


Figure 13: Schematic illustration of the in-situ HEXRD experimental setup.

3.5 Mechanical characterisation

3.5.1 Uniaxial tensile test

Uniaxial tensile testing was performed to determine the tensile parameters of the steels, such as yield strength, ultimate tensile strength, and total elongation at fracture. The tensile properties of the heat-treated samples were evaluated using a Dartec universal tensile test machine. An extensometer with a 50 mm gauge length was used to measure the total relative elongation of the region of interest.

3.5.2 Fracture toughness test

Fracture toughness of thin sheets under plane stress conditions is known to be influenced by specimen thickness due to changes in the crack-tip stress state and associated plastic deformation. To enable a meaningful comparison of fracture toughness between the investigated steel grades, all specimens were prepared to the same thickness. The PHS2000 grade, initially supplied with a slightly larger thickness (3 mm), was therefore ground to a final thickness of 2.5 mm. This ensured consistent test geometry and minimised thickness-related effects on the measured fracture toughness.

The fracture toughness was assessed by means of J-integral measurements and the essential work of fracture tests. For the J-integral measurements, the compact tension C(T) specimen geometry was used (Figure 14). The tests began with fatigue pre-cracking to propagate a crack at the tip of the notch of the sample. The C(T) specimens were inserted into a universal tensile testing machine and subjected to fracture, with the load vs displacement curves being recorded throughout the process. The displacement was measured using a clip-gage extensometer. A high-resolution video camera, synchronised on one side of the specimen, was utilised to monitor the crack extension (Δa) at the surface. The J-integral curves were then created for each material, following the methodology outlined in ASTM E1820 [121].

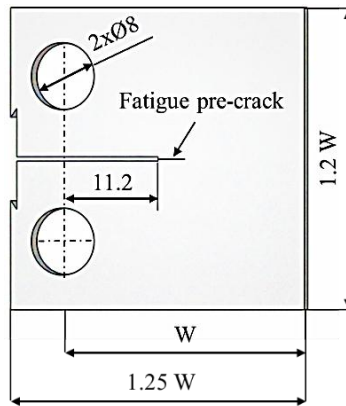


Figure 14: C(T) specimen geometry used for J-integral measurements ($W = 32$ mm).

3.5.3 Three-point bending

Bending tests were performed in accordance with the VDA 238-100 standard [122], with a modification to the specimen width, which was reduced from 30 mm to 20 mm due to limitations of the load cell. Specimens for the three-point bending test were machined to dimensions of 60×20 mm², with the bend axis aligned parallel to the rolling direction.

3.5.4 Hardness

Hardness measurements were performed using a Struers Duramin 40 microhardness tester equipped with a Vickers indenter, applying a load of 1 kg.

Chapter 4 Summary of Appended Papers

4.1 Paper I

Effect of tempering on microstructure and tensile properties of ultra-high strength steels for press hardening applications

Khalifa Maissara, Farnoosh Forouzan, Pia Åkerfeldt, Ilana Timokhina, Paul Åkerström, Esa Vuorinen, Marta-Lena Antti

Metallurgical and Materials Transactions A 56.7 (2025): 2570-2585.

This study examined the impact of tempering and auto-tempering parameters on the mechanical properties and microstructure evolution of ultra-high-strength steels, PHS1500 and PHS2000, intended for press hardening applications. The tempering process was conducted based on the low-temperature tempering conditions typical of automobile parts baking treatments, at four different temperatures and holding times. The auto-tempering experiments were conducted by varying the cooling conditions during press quenching, specifically through different dwell times in the forming tools, allowing tempering to occur inherently during the quenching stage. The results showed that tempering temperature had a stronger influence on the mechanical properties than tempering time (Figure 15). Low-temperature tempering (180-200 °C) increased the yield strength while preserving the high ultimate tensile strength and ductility of the steels. In contrast, higher tempering temperatures (≥ 250 °C) promoted martensite recovery and carbide coarsening, leading to a reduction in strength and, at 300 °C, a pronounced effect of tempered martensite embrittlement. Microstructural observations confirmed that these changes were associated with iron carbide precipitation and a reduction in dislocation density. The auto-tempering results confirmed that partial tempering occurs already during quenching, leading to the formation of fine carbides. The study also demonstrated that auto-tempering during press hardening can produce comparable property trends to conventional quenching and tempering treatments.

These findings highlighted that low-temperature tempering provides an optimal combination of high strength and ductility for both steels, while higher tempering

temperatures should be avoided due to pronounced softening and embrittlement effects associated with cementite formation.

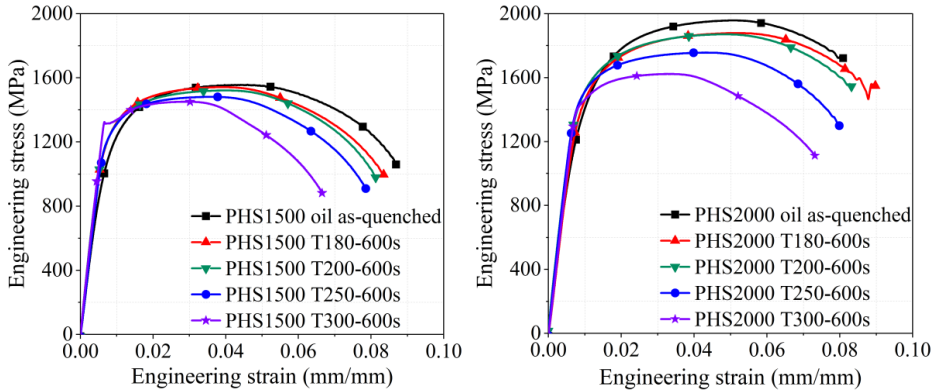


Figure 15: Engineering stress-strain curves of PHS1500 (left) and PHS2000 (right) in the as-quenched condition and after tempering at different temperatures (180-300 °C for 600 s), highlighting the effect of temperature on strength and ductility.

Contributions: The author conducted the experimental work, performed the mechanical testing and microstructural analysis, analysed the data, and wrote the paper with input and suggestions from co-authors.

4.2 Paper II

Effect of paint baking on the fracture resistance of a 2 GPa press-hardened steel used in automotive applications

Khalifa Maissara, Simon Larsson, Farnoosh Forouzan, Erik Olsson, Pia Åkerfeldt, Paul Åkerström, Ilana Timokhina, Marta-Lena Antti

Manuscript submitted to Materials Processing Technology.

This study investigated the fracture resistance of press-hardened steels with nominal strength levels of 1.5 GPa and 2.0 GPa, with particular focus on the effect of paint baking treatment. Fracture toughness was evaluated using J-R curve measurements on sheet specimens with thicknesses of 2.5-3.0 mm in the press-hardened condition and after a baking treatment representative of industrial paint-bake cycles. Complementary microstructural characterisations were performed using SEM, EBSD, and EDS, together with tensile and bending tests. All investigated

steels exhibited martensitic microstructures after press hardening. Due to the relatively high martensite start and finish temperatures, auto-tempering occurred during quenching, resulting in the formation of fine iron carbides within the martensite laths. The results showed that increasing the strength level from 1.5 to 2.0 GPa led to a pronounced reduction in fracture resistance. Baking treatment improved fracture resistance for all steels, with a more significant effect observed in the 2 GPa steels, which was attributed to low-temperature tempering and associated microstructural relaxation. Within the 2 GPa strength class, prior austenite grain size had a modest but systematic influence, with finer grains providing consistently higher resistance to crack propagation over the entire crack extension range. The bending results showed that the higher-strength steel exhibited higher load-bearing capacity but reduced bending angles, indicating a lower capacity for localised deformation. This behaviour was consistent with the reduced crack-growth resistance observed in the fracture toughness tests.

Overall, the study demonstrated that strength level is the dominant factor governing fracture behaviour in press-hardened steels at ultra-high strength levels, while baking treatment contributed beneficially to crack-growth resistance.

Contributions: The author conducted the experimental work, performed the tensile tests, actively participated in the fracture toughness tests, carried out the microstructural analysis and fractography, processed the fracture toughness and bending test data, analysed the results, and wrote the paper with input and suggestions from co-authors. The press hardening treatment and bending tests were carried out by the research team at Gestamp HardTech.

4.3 Paper III

Effect of thermomechanical treatment on phase transformation kinetics during press hardening process

Khalifa Maissara, Farnoosh Forouzan, Paul Åkerström, Pia Åkerfeldt, Ilana Timokhina, Marta-Lena Antti

Manuscript.

This study investigated the influence of deformation on phase transformation behaviour in a 2 GPa press-hardening steel under isothermal conditions. The work aimed to improve the understanding of deformation-transformation interactions during press hardening, which are critical for controlling the final microstructure and mechanical properties of ultra-high-strength steels. Thermomechanical experiments were conducted using a Gleeble simulator, where deformation was applied at elevated temperatures followed by continuous cooling. The effects of deformation amount, strain rate, and deformation temperature were systematically evaluated. The transformation behaviour during cooling was characterised using dilatometry and correlated with microstructural observations and hardness measurements. The results showed that deformation significantly influences phase transformation. Increasing the deformation amount promoted diffusional transformation, leading to the formation of diffusional phases and a corresponding reduction in the martensite fraction. Deformation temperature had a strong effect: lower deformation temperatures enhanced diffusional transformation, while higher temperatures resulted in predominantly martensitic microstructures. These transformation trends were reflected in the hardness measurements. Increased deformation led to reduced hardness due to the formation of diffusional transformation products, whereas higher deformation temperatures produced hardness values close to the as-quenched condition.

Contributions: The author conducted the thermomechanical processing, performed microstructural analysis, analysed the data, and wrote the paper with input and suggestions from co-authors.

4.4 Paper IV

The influence of austenitization conditions on grain growth and the bending performance of boron steel

Erik Lundholm, Khalifa Maissara, Paul Åkerström

Materials and Metallurgical Transactions B 57.1 (2026): 552-563.

This paper investigated the effect of austenitization conditions on the evolution of the parent austenite grain size (PAGS) and its influence on the bending performance of press-hardened PHS1500 boron steel (22MnB5). The work focused on both the modelling of grain growth during austenitization and the experimental evaluation of the mechanical response after quenching and baking. Austenite grain growth was studied using isothermal heat treatments in the range 900-960 °C with holding times between 1 and 1200 s. The resulting grain sizes were used to develop a grain growth model based on the evolution of the mean grain diameter. The results showed that grain growth increases with both temperature and holding time, but remains limited at 900 °C. At higher temperatures, particularly at 960 °C, the microstructure becomes inhomogeneous, exhibiting indications of abnormal grain growth. The proposed model accurately predicted grain growth under conditions where the microstructure remains homogeneous, but showed deviations at higher temperatures. Bending performance was evaluated using VDA 238-100 tests. For short austenitization times, no significant effect of austenitization temperature on bending behaviour was observed. However, at longer holding times and higher temperatures, a slight decrease in bending performance was detected, associated with increased grain size.

This study demonstrated that austenite grain growth can be predicted from the thermal history under conditions of homogeneous growth, providing a basis for improved process modelling in press hardening, while highlighting the limitations of inhomogeneous microstructure evolution at elevated temperatures.

Contributions: The author performed part of the microstructural analysis and wrote the corresponding section, conducted hardness testing, and contributed to manuscript proofreading and revision. The parent austenite grain size evaluation was carried out by Swerim AB.

4.5 Paper V

Influence of pre-existing martensite on the acceleration of carbide-free bainite transformation studied by in-situ synchrotron XRD

Khalifa Maissara, Farnoosh Forouzan, Roohallah Surki Aliabad, Emad Maawad, Esa Vuorinen
Manuscript under review at Materials Today Communications.

This study evaluated the role of pre-existing martensite in governing the kinetics and mechanisms of carbide-free bainitic transformation in a low-carbon, high-silicon steel (0.2 wt.% C-1.5 wt.% Si). A unified experimental framework was employed to directly compare quenching and partitioning (Q&P), single-step austempering, and two-step austempering under identical thermal histories. The phase evolution during quenching, reheating, isothermal holding, and final cooling was continuously monitored using in-situ high-energy X-ray diffraction (HEXRD), enabling quantitative tracking of austenite fraction and carbon enrichment. The results demonstrated that the transformation pathway was strongly controlled by the quench temperature relative to the martensite start temperature (M_s) (Figure 16). When quenching below M_s , the formation of supersaturated martensite prior to the isothermal stage significantly accelerated bainitic transformation. This acceleration was attributed to the increased density of interfaces, which promoted bainite nucleation. Complementary EBSD analysis of the final microstructures showed a significantly higher grain boundary density in martensite-containing conditions, supporting an interface-controlled contribution to the accelerated transformation kinetics. Under these conditions, carbon partitioning from martensite to austenite occurred rapidly, leading to early and effective stabilisation of retained austenite within a few tens of seconds. In contrast, austempering routes, initiated above M_s , proceed through bainite formation in a fully austenitic microstructure, resulting in slower transformation kinetics, delayed carbon enrichment, and a heterogeneous distribution of carbon in austenite. At higher transformation temperatures, this leads to incomplete stabilisation within the applied holding times.

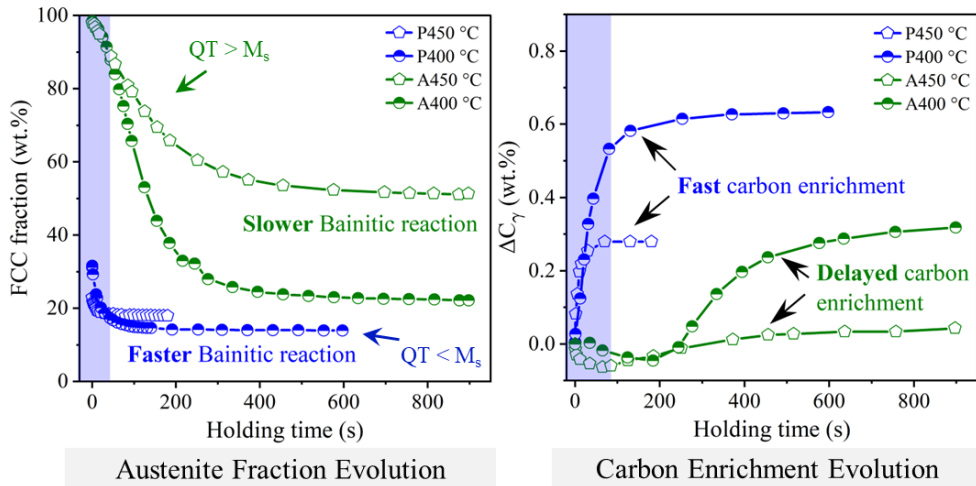


Figure 16: Effect of quench temperature relative to M_s on transformation kinetics and carbon enrichment. Martensite-assisted conditions ($QT < M_s$) show accelerated bainite formation and rapid carbon enrichment, whereas austempering conditions ($QT > M_s$) exhibit slower transformation and delayed carbon redistribution.

Contributions: The author performed the data analysis and interpretation of the in-situ synchrotron X-ray diffraction results, conducted microstructural characterisation, and wrote the paper with input and suggestions from co-authors.

Chapter 5 Conclusions and Future Work

5.1 Conclusions

This thesis investigated the process-structure-property relationships governing the performance of ultra-high strength press hardening steels, with particular emphasis on commercially available 2.0 GPa grade steel benchmarked against the conventional 1.5 GPa grade. The work spans the press hardening value chain, from austenitization and thermomechanical processing through phase transformation, post-quench thermal treatment, as well as alternative microstructure design routes via quenching and partitioning. The main conclusions drawn from the thesis work are summarised below.

How do tempering and auto-tempering influence the tensile properties and fracture toughness of different grades of press-hardening steels?

Tempering temperature played a greater role than tempering time in shaping the mechanical properties of press-hardened steels. Optimal results were achieved with low-temperature tempering at 180-200 °C, increasing yield strength while preserving both the high tensile strength and ductility. This improvement was associated with iron carbide precipitation and a partial reduction in dislocation density, thereby relieving residual stresses without compromising strength. At higher tempering temperatures of 250-300 °C, martensite recovery and carbide coarsening became dominant, causing a pronounced reduction in strength. At 300 °C, tempered martensite embrittlement was more evident, driven by the formation and coarsening of cementite along lath and prior austenite grain boundaries. In the press hardening route, moderate auto-tempering at ejection temperatures of 150-200 °C yielded the optimal strength-ductility balance, while ejection at 300 °C caused embrittlement similar to that seen in conventional quenching and tempering, again due to cementite formation.

Fracture resistance was found to be primarily governed by carbon content and strength level. The 2 GPa grade, with its higher carbon content, exhibited significantly lower fracture resistance compared to the 1.5 GPa steel. Importantly, paint baking treatment of 175 °C/20 min, significantly improved fracture resistance in

the 2 GPa grade, with $J_{0.2}$ increasing by 54%, an effect considerably more pronounced than in the 1.5 GPa steel. Within the 2 GPa grade, finer prior austenite grains provided a modest but consistent improvement in crack growth resistance.

How do austenitization parameters and prior austenite deformation influence the evolution of parent austenite and its impact on phase transformation and mechanical performance in press-hardening steels?

Prior austenite deformation induced diffusive transformation under all investigated conditions, with the combined ferrite and bainite fraction ranging from approximately 4% to 41%, depending on deformation conditions. Deformation temperature emerged as the most critical parameter, with a sharp transition in transformation behaviour observed below 760 °C. The increased fraction of diffusive transformation products was directly reflected in the hardness of the final microstructure, with hardness decreasing systematically as deformation strain increases and deformation temperature decreases. In addition, deformation was found to reduce the martensite start temperature by up to 33 °C relative to the non-deformed condition. These results have direct implications for industrial press hardening of the 2 GPa grade, where achieving a fully martensitic microstructure requires careful control of both forming temperature and strain distribution across the part geometry.

Austenite grain growth during austenitization increased with both temperature and holding time. Growth remained limited at 900 °C but accelerated markedly at 960 °C, where indications of abnormal grain growth were observed. A grain growth model based on the evolution of mean grain diameter was developed. The model could successfully predict grain growth under conditions of homogeneous growth, while deviating at higher temperatures where abnormal growth occurs. Austenitization temperature had no significant effect on bending performance for short holding times, while only a minor reduction was observed at longer holding times combined with elevated temperatures.

How does pre-existing martensite influence the kinetics and mechanism of carbide-free bainitic transformation during quenching and partitioning heat treatment?

The quench temperature relative to the martensite start temperature was identified as the critical parameter controlling the transformation pathway during Q&P treatment. Pre-existing martensite, formed by quenching below M_s temperature, accelerated carbide-free bainitic transformation and promoted rapid carbon partitioning to austenite, leading to earlier and more effective retained austenite stabilisation compared to austempering routes initiated above M_s . The higher amount of interfaces in martensite-containing microstructures was identified as the primary factor promoting this acceleration. Taken together, these results demonstrated that the quench temperature, through its control of the initial martensite fraction, governs both the kinetics of bainite transformation and the extent of carbon partitioning during the Q&P treatment. This is particularly important for press hardening applications, where achieving sufficient retained austenite stabilisation within short processing windows is critical for the design of Q&P-based thermal cycles.

5.2 Future work

The findings of this thesis open several research directions for further investigations:

The results of Paper II demonstrated that paint baking treatment improved the fracture resistance of the 2 GPa grade, and this improvement was attributed to relaxation of residual stresses. However, no dedicated characterisation was performed to directly verify this mechanism. Future work should therefore include targeted experimental investigation, such as residual stress measurements before and after baking, to confirm and quantify the contribution of stress relaxation to the observed improvement in fracture toughness.

Furthermore, the effect of prior austenite grain size on fracture resistance was found to be modest when assessed using J-R curve measurements on compact tension specimens, despite the expectation of a more pronounced effect given the large difference in grain size between the two investigated conditions. However,

drawing strong conclusions regarding the crack propagation resistance can be difficult due to the possibility of additional energy from plastic work using J-integral measurements. Two different steel grades can show similar J-R curves but have different energy contributions [111] for the same crack advance. This is due to the fact that the J-integral approach incorporates both the essential and non-essential components of the work of fracture. The essential work of fracture method, which separates the essential work consumed in the fracture process zone from the outer plastic dissipation, may provide a more discriminating assessment of the role of prior austenite grain size on fracture resistance in these steels. This approach has been successfully applied to advanced high-strength steel sheets and press-hardened steels by other researchers and applying it to the grades investigated in this thesis, particularly comparing fine and coarse prior austenite grain conditions in the 2 GPa grade, represents a promising extension of the present work. Due to the good correlation between crash performance and fracture toughness measured using the essential work of fracture method [109], the influence of the paint baking treatment on fracture toughness of these ultra-high-strength grades is interesting from a passenger safety point-of-view.

Regarding the effect of prior austenite deformation on phase transformation kinetics studied in Paper III, all experiments were conducted under one single cooling rate (~ 55 °C/s) following isothermal deformation. Investigating the effect of deformation under a range of cooling rates would enable the construction of deformation-corrected continuous cooling transformation diagrams, revealing how deformation shifts the ferrite and bainite transformation noses to shorter durations. Such data would significantly enrich the current understanding of deformation-transformation interactions and provide the quantitative input needed to incorporate deformation effects into existing phase transformation models used for press hardening simulation. Validation of such models against measurements on a press-hardened component would be a valuable further step, bridging the gap between laboratory-scale Gleeble experiments and industrial press hardening conditions.

The results presented in Paper V indicate that quenching and partitioning (Q&P) is a promising approach for introducing TRIP-assisted microstructures into press-hardening steels beyond fully martensitic grades. However, the potential of this

process should be further investigated through detailed microstructural characterisation and mechanical performance evaluation. Since crash performance is a critical requirement for press-hardened steels, the stabilisation of retained austenite through Q&P processing may be beneficial, as retained austenite can hinder crack propagation in the martensitic matrix.

References

- [1] O. Bouaziz, H. Zurob, M. Huang, Driving force and logic of development of advanced high strength steels for automotive applications, *Steel Res. Int.* 84 (2013) 937–947.
- [2] S.A. Pradeep, R.K. Iyer, H. Kazan, S. Pilla, Automotive Applications of Plastics: Past, Present, and Future, in: *Applied Plastics Engineering Handbook*, 2nd ed., William Andrew Publishing, (2017) 651–673.
- [3] A. Kelkar, R. Roth, J. Clark, Automobile Bodies: Can Aluminum Be an Economical Alternative to Steel?, *JOM* 53 (2001) 28–32.
- [4] E. Billur, *Hot Stamping of Ultra High-Strength Steels From a technological and business perspective*, Springer Cham, 2019.
- [5] D. Ivkovic, D. Adamovic, A. Dusan, N. Ratkovic, R. Nikolic, Review of the first generation of the advanced high-strength steels (AHSS) and their manufacturing procedures, 39th Int Conf on Production Engineering of Serbia, (2023) 181-188.
- [6] Y.K. Lee, J. Han, Current Opinion in Medium-Manganese Steel, *Mater. Sci. Technol.* 31 (2015) 843–856.
- [7] D.K. Matlock, J.G. Speer, Third Generation of AHSS: Microstructure Design Concepts, In *Microstructure and Texture in Steels and Other Materials*, Springer, (2009) 185-205.
- [8] S. Kumar, S.B. Singh, Quenching and Partitioning (Q&P) Steel: Alloy Design, Phase Transformation and Evolution of Microstructure, *Metall. Mater. Trans. A* 54 (2023) 3134–3156.
- [9] T. Taylor, A. Clough, Critical review of automotive hot-stamped sheet steel from an industrial perspective, *Mater. Sci. Technol.* 34 (2018) 809–861.
- [10] J. Li, C. Tong, R. Zhang, Z. Shi, J. Lin, A data-informed review of scientific and technological developments and future trends in hot stamping, *Int. J. Lightweight Mater. Manuf.* 7 (2024) 327–343.

- [11] M. Naderi, A. Saeed-Akbari, W. Bleck, The effects of non-isothermal deformation on martensitic transformation in 22MnB5 steel, *Mater. Sci. Eng. A* 487 (2008) 445–455.
- [12] Y. Li, Y. Chen, S. Li, Phase transformation testing and modeling for hot stamping of boron steel considering the effect of the prior austenite deformation, *Mater. Sci. Eng. A* 821 (2021) 141447.
- [13] G. Berglund, The history of hardening of boron steel in northern Sweden, In 1st Int Conf on Hot Sheet Metal Forming of High-Performance Steel, (2008) 175–177.
- [14] D.W. Fan, and B.C. De Cooman, State-of-the-knowledge on coating systems for hot stamped parts, *Steel Res. Int.* 83 (2012) 412–433.
- [15] L.M. Arias, G. Artola, I. Porto, Hot Stamping Research Scenarios from the Last Decade, *Mater. Proc.* 3 (2021) 26.
- [16] H. Karbasian, A.E. Tekkaya, A review on hot stamping, *J. Mater. Process. Technol.* 210 (2010) 2103–2118.
- [17] Z. Cheng, M. Gao, J. Liu, S. Wang, G. Wu, J. Gao, H. Wu, X. Mao, Multi-Scale Microstructural Tailoring and Associated Properties of Press-Hardened Steels: A Review, *Materials* 16 (2023) 3799.
- [18] K. Mori, P.F. Bariani, B.A. Behrens, A. Brosius, S. Bruschi, T. Maeno, M. Merklein, J. Yanagimoto, Hot stamping of ultra-high strength steel parts, *CIRP Ann. Manuf. Technol.* 66 (2017) 755–777.
- [19] W. Bleck, S. Bruhl, T. Gerber, A. Katsamas, R. Ottaviani, L. Samek, S. Traint, Control and exploitation of the bake-hardening effect in multi-phase high-strength steels, *EUR* 22448 (2007) 1-169.
- [20] D.W. Fan, H.S. Kim, B.C. De Cooman, A Review of the Physical Metallurgy related to the Hot Press Forming of Advanced High Strength Steel, *Steel Res. Int.* 80 (2009) 241-248.
- [21] H. Järvinen, M. Honkanen, M. Järvenpää, P. Peura, Effect of paint baking treatment on the properties of press hardened boron steels, *J. Mater. Process. Technol.* 252 (2018) 90–104.

-
- [22] D.A. Porter, K.E. Easterling, M.Y. Sherif, *Phase Transformations in Metals and Alloys*, 4th ed., CRC Press, 2022.
- [23] D. Koistinen, R. Marburger, J.R. Low, A general equation prescribing the extent of the austenite-martensite transformation in pure iron-carbon alloys and plain carbon steels, *Acta Metall.* 7 (1959) 59–60.
- [24] Y. Li, M. Xu, Y. Jin, H. Lu, Finite-element simulation of low-alloy high strength steel welding incorporating improved martensite transformation kinetics and recrystallization annealing, *ISIJ Int.* 55 (2015) 1448–1453.
- [25] G.R. Speich, W.C. Leslie, Tempering of Steel, *Metall. Trans.* 3 (1972) 1043–1054.
- [26] M. Naderi, M. Abbasi, A. Saeed-Akbari, Enhanced mechanical properties of a hot-stamped advanced high-strength steel via tempering treatment, *Metall. Mater. Trans. A* 44 (2013) 1852–1861.
- [27] O. Haiko, A. Kaijalainen, S. Pallaspuuro, J. Hannula, D. Porter, T. Liimatainen, J. Kömi, The effect of tempering on the microstructure and mechanical properties of a novel 0.4C press-hardening steel, *Appl. Sci.* 9 (2019) 4231.
- [28] O. Cavusoglu, O. Cavusoglu, A.G. Yilmazoglu, U. Uzel, H. Aydin, A. Güral, Microstructural features and mechanical properties of 22MnB5 hot stamping steel in different heat treatment conditions, *J. Mater. Res. Technol.* 9 (2020) 10901–10908.
- [29] Y. Hirotsu, S. Nagakura, Electron Microscopy and Diffraction Study of the Carbide Precipitated at the First Stage of Tempering of Martensitic Medium Carbon Steel, *Trans. Jpn. Inst. Met.* 15 (1974) 129–134.
- [30] G. Krauss, Tempering of Lath Martensite in Low and Medium Carbon Steels: Assessment and Challenges, *Steel Res. Int.* 88 (2017) 1700038.
- [31] B. Hutchinson, D. Lindell, M. Barnett, Yielding behaviour of martensite in steel, *ISIJ Int.* 55 (2015) 1114–1122.

- [32] L. Cheng, C.M. Brakman, B.M. Korevaar, E.J. Mittemeijer, The Tempering of Iron-Carbon Martensite; Dilatometric and Calorimetric Analysis, *Metall. Trans. A* 19 (1988) 2415–2426.
- [33] G. Krauss, Tempering of martensite in carbon steels, in: *Phase Transformations in Steels*, Woodhead Publishing, (2012) 126–150.
- [34] W.-S. Lee, T.-T. Su, Mechanical properties and microstructural features of AISI 4340 high-strength alloy steel under quenched and tempered conditions, *J. Mater. Process. Technol.* 87 (1999) 198–206.
- [35] T. Swarr, G. Krauss, The Effect of Structure on the Deformation of As-Quenched and Tempered Martensite in an Fe-0.2 Pct C Alloy, *Metallur. Trans. A* 7 (1976) 41–48.
- [36] D.L. Williamson, R.G. Schupmann, J.P. Materkowski, G. Krauss, Determination of Small Amounts of Austenite and Carbide in Hardened Medium Carbon Steels by Mössbauer Spectroscopy, *Metallur. Trans. A* 10 (1979) 379–382.
- [37] H.J. Kim, H.K. Park, C.W. Lee, B.G. Yoo, H.Y. Jung, Baking effect on desorption of diffusible hydrogen and hydrogen embrittlement on hot-stamped boron martensitic steel, *Metals*. 9 (2019) 636.
- [38] S. Lee, J. Ronevich, G. Krauss, D. Matlock, Hydrogen Embrittlement of Hardened Low-carbon Sheet Steel, *ISIJ Int.* 50 (2010) 294–301.
- [39] J. Venezuela, Q. Zhou, Q. Liu, H. Li, M. Zhang, M.S. Dargusch, A. Atrens, The influence of microstructure on the hydrogen embrittlement susceptibility of martensitic advanced high strength steels, *Mater. Today Commun.* 17 (2018) 1–14.
- [40] G. Lovicu, M. Bottazzi, F. D'aiuto, M. De Sanctis, A. Dimatteo, C. Santus, R. Valentini, Hydrogen embrittlement of automotive advanced high-strength steels, *Metall. Mater. Trans. A* 43 (2012) 4075–4087.
- [41] H.K.D.H. Bhadeshia, Prevention of Hydrogen Embrittlement in Steels, *ISIJ Int.* 56 (2016) 24–36.

- [42] C. Georges, T. Sturel, P. Drillet, J.M. Mataigne, Absorption/desorption of diffusible hydrogen in aluminized boron steel, *ISIJ Int.* 53 (2013) 1295–1304.
- [43] B. Jian, L. Wang, H. Mohrbacher, H.Z. Lu, W.J. Wang, Development of Niobium Alloyed Press Hardening Steel with Improved Properties for Crash Performance, *Adv. Mater. Res.* 1063 (2014) 7–20.
- [44] L.C.F. Canale, J. Vatauvuk, G.E. Totten, Introduction to Steel Heat Treatment, in: *Comprehensive Materials Processing*, Elsevier (2014) 3-37.
- [45] H. Bhadeshia, R. Honeycombe, Heat Treatment of Steels: Hardenability, in: *Steels: Microstructure and Properties*, Elsevier (2017) 217–236.
- [46] A. Fadel, D. Glišić, N. Radović, D. Drobñjak, Influence of Cr, Mn and Mo Addition on Structure and Properties of V Microalloyed Medium Carbon Steels, *J. Mater. Sci. Technol.* 28 (2012) 1053–1058.
- [47] M. Ueno, T. Inoue, Distribution of Boron at Austenite Grain Boundaries and Bainitic Transformation in Low Carbon Steels, *Trans. Iron Steel Inst. Jpn.* 13 (1973) 210–217.
- [48] C.A. Suski, C.A.S. Oliveira, Effect of Austenitization Temperature on the Precipitation of Carbides in Quenched Low Carbon Boron Steel, *Metallogr. Microstruct. Anal.* 2 (2013) 79–87.
- [49] Y. Zheng, L. Zhang, Y. Lin, J. Wang, K. Wang, Z. Guo, R. Cao, L. Zhu, B. Wang, D. Zhang, J. Feng, Effect of compound addition of Ti–B on hardenability and hot ductility of 22MnB5 hot stamped steel, *J. Mater. Res. Technol.* 36 (2025) 1173–1193.
- [50] M. Saeglitz, G. Krauss, Deformation, Fracture, and Mechanical Properties of Low-Temperature-Tempered Martensite in SAE 43xx Steels, *Metall. Mater. Trans. A* 28 (1997) 377–387.
- [51] G. Krauss, Deformation and Fracture in Martensitic Carbon Steels Tempered at Low Temperatures, *Metall. Mater. Trans. A* 32 (2001) 861–877.
- [52] S. Morito, J. Nishikawa, T. Maki, Dislocation Density within Lath Martensite in Fe-C and Fe-Ni Alloys, *ISIJ Int.* 43 (2003) 1475–1477.

- [53] S. Takebayashi, T. Kunieda, N. Yoshinaga, K. Ushioda, S. Ogata, Comparison of the Dislocation Density in Martensitic Steels Evaluated by Some X-ray Diffraction Methods, *ISIJ Int.* 50 (2010) 875-882.
- [54] T. Taylor, G. Fourlaris, A. Clough, Effect of carbon and microalloy additions on hot-stamped boron steel, *Mater. Sci. Technol.* 33 (2017) 1964–1977.
- [55] T. Taylor, S. Danks, G. Fourlaris, Dynamic Tensile Testing of Ultrahigh Strength Hot Stamped Martensitic Steels, *Steel Res. Int.* 88 (2017) 1600144.
- [56] M. Shamsujjoha, Evolution of microstructures, dislocation density and arrangement during deformation of low carbon lath martensitic steels, *Mater. Sci. Eng. A* 776 (2020) 139039.
- [57] T. Tanaka, N. Maruyama, N. Nakamura, A.J. Wilkinson, Tetragonality of Fe-C martensite – a pattern matching electron backscatter diffraction analysis compared to X-ray diffraction, *Acta Mater.* 195 (2020) 728–738.
- [58] Y. Lu, H. Yu, R.D. Sisson, The effect of carbon content on the c/a ratio of as-quenched martensite in Fe-C alloys, *Mater. Sci. Eng. A* 700 (2017) 592–597.
- [59] G. Krauss, Tempering of martensite in carbon steels, in: *Phase Transformations in Steels*, Woodhead Publishing, (2012) 126–150.
- [60] V. Javaheri, S. Pallaspuuro, S. Sadeghpour, S. Ghosh, J. Sainio, R. Latypova, J. Kömi, Rapid tempering of a medium-carbon martensitic steel: In-depth exploration of the microstructure – mechanical property evolution, *Mater. Des.* 231 (2023) 112059.
- [61] R. Rana, S.B. Singh, *Automotive Steels: Design, Metallurgy, Processing and Applications*, Woodhead Publishing, 2016.
- [62] L.J. Baker, S.R. Daniel, J.D. Parker, Metallurgy and processing of ultralow carbon bake hardening steels, *Mater. Sci. Technol.* 18 (2002) 355–368.
- [63] O.G. Kumpyak, Z.R. Galyautdinov, D.R. Galyautdinov, H. Bartkova, M. Paidar, K. Bouzek, Dislocation Theory of Yielding and Strain Ageing of Iron, *Proc. Phys. Soc., Sect. A* 62 (1949) 49-62.

-
- [64] D. V Wilson, B. Russell, The contribution of atmosphere locking to the strain-ageing of low carbon steels, *Acta Metall.* 8 (1960) 36–45.
- [65] D. V Wilson, B. Russell, The contribution of precipitation to strain ageing in low carbon steels, *Acta Metall.* 8 (1960) 468–479.
- [66] G. Badinier, C.W. Sinclair, X. Sauvage, X. Wang, V. Bylik, M. Gouné, F. Danoix, Microstructural heterogeneity and its relationship to the strength of martensite, *Mater. Sci. Eng. A* 638 (2015) 329–339.
- [67] J. Wilde, A. Cerezo, G.D.W. Smith, Three-dimensional atomic-scale mapping of a Cottrell atmosphere around a dislocation in iron, *Scr. Mater.* 43 (2000) 39–48.
- [68] I.B. Timokhina, P.D. Hodgson, S.P. Ringer, R.K. Zheng, E. V Pereloma, Understanding bake-hardening in modern high strength steels for the automotive industry using advanced analytical techniques, In *Proc Int Conf New Developments on Metallurgy and Applications of High Strength Steels*, 2008.
- [69] G. Krauss, Heat treated martensitic steels: microstructural systems for advanced manufacture, *ISIJ Int.* 35 (1995) 349–359.
- [70] J. Speer, D.K. Matlock, B.C. De Cooman, J.G. Schroth, Carbon partitioning into austenite after martensite transformation, *Acta Mater.* 51 (2003) 2611–2622.
- [71] J.G. Speer, F.C. Rizzo Assunção, D.K. Matlock, D. V Edmonds, The “Quenching and Partitioning” Process: Background and Recent Progress, *Mater Res* 8 (2005) 417–423.
- [72] A.J. Clarke, J.G. Speer, D.K. Matlock, F.C. Rizzo, D. V. Edmonds, M.J. Santofimia, Influence of carbon partitioning kinetics on final austenite fraction during quenching and partitioning, *Scr Mater.* 61 (2009) 149–152.
- [73] R.A. Stewart, J.G. Speer, B.G. Thomas, E. De Moor, A.J. Clarke, Quenching and Partitioning of Plate Steels: Partitioning Design Methodology, *Metall. Mater. Trans. A* 50 (2019) 4701–4713.

- [74] E.J. Seo, L. Cho, B.C. De Cooman, Application of quenching and partitioning (Q&P) processing to press hardening steel, *Metall. Mater. Trans. A* 45 (2014) 4022–4037.
- [75] E.P. Vuorinen, A.G. Ozugurler, J.C. Ion, K. Eriksson, M.C. Somani, L.P. Karjalainen, S. Allain, F.G. Caballero, Hot forming of ultra-fine-grained multiphase steel products using press hardening combined with quenching and partitioning process, *Metals*. 9 (2019) 357.
- [76] E.A.A. Echeverri, A.S. Nishikawa, M. Masoumi, H.B. Pereira, N.G. Marulanda, A.M. Rossy, H. Goldenstein, A.P. Tschiptschin, In Situ Synchrotron X-ray Diffraction and Microstructural Studies on Cold and Hot Stamping Combined with Quenching and Partitioning Processing for Development of Third-Generation Advanced High Strength Steels, *Metals*. 12 (2022) 174.
- [77] H. Liu, X. Jin, H. Dong, J. Shi, Martensitic microstructural transformations from the hot stamping, quenching and partitioning process, *Mater. Charact.* 62 (2011) 223–227.
- [78] H. Liu, X. Lu, X. Jin, H. Dong, J. Shi, Enhanced mechanical properties of a hot stamped advanced high-strength steel treated by quenching and partitioning process, *Scr. Mater.* 64 (2011) 749–752.
- [79] B.C. De Cooman, Structure-properties relationship in TRIP steels containing carbide-free bainite, *Curr. Opin. Solid State Mater. Sci.* 8 (2004) 285–303.
- [80] F.G. Caballero, S. Allain, J. Cornide, J.D. Puerta Velásquez, C. Garcia-Mateo, M.K. Miller, Design of cold rolled and continuous annealed carbide-free bainitic steels for automotive application, *Mater. Des.* 49 (2013) 667–680.
- [81] W. Bleck, X. Guo, Y. Ma, The TRIP Effect and Its Application in Cold Formable Sheet Steels, *Steel Res. Int.* 88 (2017) 1700218.
- [82] V.L. Nuam, H. Zhang, Y.C. Wang, Z.P. Xiong, Role of retained austenite in advanced high-strength steel: ductility and toughness, *J. Iron Steel Res. Int.* 31 (2024) 2079–2089.

-
- [83] C. Hu, C.P. Huang, Y.X. Liu, A. Perlade, K.Y. Zhu, M.X. Huang, The dual role of TRIP effect on ductility and toughness of a medium Mn steel, *Acta Mater.* 245 (2023) 118629.
- [84] S. Ebner, R. Schnitzer, E. Maawad, C. Suppan, C. Hofer, Influence of partitioning parameters on the mechanical stability of austenite in a Q&P steel: A comparative in-situ study, *Materialia*. 15 (2021) 101033.
- [85] P. Huyghe, M. Caruso, J.L. Collet, S. Dépinoy, S. Godet, Into the quenching and; partitioning of a 0.2C steel: An in-situ synchrotron study, *Mater. Sci. Eng. A* 743 (2019) 175–184.
- [86] S.Y.P. Allain, G. Geandier, J.C. Hell, M. Soler, F. Danoix, M. Gouné, In-situ investigation of quenching and partitioning by High Energy X-Ray Diffraction experiments, *Scr. Mater.* 131 (2017) 15–18.
- [87] S.Y.P. Allain, G. Geandier, J.C. Hell, M. Soler, F. Danoix, M. Gouné, Effects of Q&P processing conditions on austenite carbon enrichment studied by in situ high-energy X-ray diffraction experiments, *Metals* 7 (2017) 232.
- [88] S. Wang, A.A. Kistanov, G. King, S. Ghosh, H. Singh, S. Pallaspuuro, A. Rahemtulla, M. Somani, J. Kömi, W. Cao, M. Huttula, In-situ quantification and density functional theory elucidation of phase transformation in carbon steel during quenching and partitioning, *Acta Mater.* 221 (2021) 117361.
- [89] S. Gaudez, J. Teixeira, S. Denis, G. Geandier, S.Y.P. Allain, Martensite and nanobainite transformations in a low alloyed steel studied by in situ high energy synchrotron diffraction, *Mater. Charact.* 185 (2022) 111740.
- [90] F. Forouzan, R. Surki Aliabad, A. Hedayati, N. Hosseini, E. Maawad, N. Blasco, E. Vuorinen, Kinetics of carbon enrichment in austenite during partitioning stage studied via in-situ synchrotron XRD, *Materials* 16 (2023) 1557.
- [91] S.Y.P. Allain, S. Gaudez, G. Geandier, F. Danoix, M. Soler, M. Goune, Carbon heterogeneities in austenite during Quenching & Partitioning (Q&P) process revealed by in situ High Energy X-Ray Diffraction (HEXRD) experiments, *Scr. Mater.* 181 (2020) 108–114.

- [92] H. Kawata, K. Hayashi, N. Sugiura, N. Yoshinaga, M. Takahashi, Effect of martensite in initial structure on bainite transformation, *Mater. Sci. Forum.* 638 (2010) 3307–3312.
- [93] A. Navarro-López, J. Sietsma, M.J. Santofimia, Effect of prior athermal martensite on the isothermal transformation kinetics below M_s in a low-C high-Si steel, *Metall. Mater. Trans. A* 47 (2016) 1028–1039.
- [94] Y. Toji, H. Matsuda, D. Raabe, Effect of Si on the acceleration of bainite transformation by pre-existing martensite, *Acta Mater.* 116 (2016) 250–262.
- [95] A.J. Clarke, J.G. Speer, M.K. Miller, R.E. Hackenberg, D. V. Edmonds, D.K. Matlock, F.C. Rizzo, K.D. Clarke, E. De Moor, Carbon partitioning to austenite from martensite or bainite during the quench and partition (Q&P) process: A critical assessment, *Acta Mater.* 56 (2008) 16–22.
- [96] Z. Shi, K. Liu, M. Wang, J. Shi, H. Dong, J. Pu, B. Chi, Y. Zhang, L. Jian, Effect of non-isothermal deformation of austenite on phase transformation and microstructure of 22SiMn2TiB steel, *Mater. Sci. Eng. A* 535 (2012) 290–296.
- [97] J. Min, J. Lin, Y. Min, F. Li, On the ferrite and bainite transformation in isothermally deformed 22MnB5 steels, *Mater. Sci. Eng. A* 550 (2012) 375–387.
- [98] S. Salari, A. Saeed-Akbari, M. Naderi, W. Bleck, Martensitic transformation behavior of b-bearing steel during isothermal deformation, *Steel Res. Int.* 83 (2012) 733–742.
- [99] P. Åkerström, M. Oldenburg, Austenite decomposition during press hardening of a boron steel-Computer simulation and test, *J. Mater. Process. Technol.* 174 (2006) 399–406.
- [100] M. Abbasi, A. Saeed-Akbari, M. Naderi, The effect of strain rate and deformation temperature on the characteristics of isothermally hot compressed boron-alloyed steel, *Mater. Sci. Eng. A* 538 (2012) 356–363.

- [101] M. Abbasi, M. Naderi, A. Saeed-Akbari, Isothermal versus non-isothermal hot compression process: A comparative study on phase transformations and structure-property relationships, *Mater. Des.* 45 (2013) 1–5.
- [102] J. Min, J. Lin, Y. Min, Effect of thermo-mechanical process on the microstructure and secondary-deformation behavior of 22MnB5 steels, *J. Mater. Process. Technol.* 213 (2013) 818–825.
- [103] S. Zuqing, Y. Wangyue, Q. Junjie, Characteristics of deformation-enhanced transformation in low carbon steel, *Mater. Sci. Forum.* 475–479 (2005) 49–54.
- [104] Y.Q. Weng, X.J. Sun, H. Dong, Deformation Induced Ferrite Transformation in Microalloyed Steels: Theory and Application, *Mater. Sci. Forum.* 561–565 (2007) 2491–2508.
- [105] J. Zhou, B.Y. Wang, M.D. WangHuang, D. Cui, Effect of hot stamping parameters on the mechanical properties and microstructure of cold-rolled 22MnB5 steel strips, *Int. J. Miner. Metall. Mater* 21 (2014) 544–555.
- [106] Z.M. Shi, J. Li, B. Chi, J. Pu, Y.S. Zhang, M.Q. Wang, J. Shi, H. Dong, Martensitic phase transformation from non-isothermally deformed austenite in high strength steel 22SiMn2TiB, *Metall. Mater. Trans. A* 44 (2013) 4136–4142.
- [107] T. Matsumoto, N. Li, X. Shi, J. Lin, An Investigation of Deformation Effects on Phase Transformation in Hot Stamping Processes, *SAE Int. J. Mater. Manuf.* 9 (2016) 501–505.
- [108] M. Li, D. Yao, B. Li, S. Yue, Z. Chen, E. Ren, N. Wang, C. Yang, Effects of Deformation Parameters on Phase Transformation of B1500HS High-Strength Steel During the Non-Isothermal Deformation Process, *Materials* 18 (2025) 2843.
- [109] D. Frómeta, A. Lara, S. Molas, D. Casellas, J. Rehrl, C. Suppan, P. Larour, J. Calvo, On the correlation between fracture toughness and crash resistance of advanced high strength steels, *Eng. Fract. Mech.* 205 (2019) 319–332.

- [110] D. Casellas, A. Lara, D. Frómeta, D. Gutiérrez, S. Molas, L. Pérez, J. Rehrl, C. Suppan, Fracture Toughness to Understand Stretch-Flangeability and Edge Cracking Resistance in AHSS, *Metall. Mater. Trans. A* 48 (2017) 86–94.
- [111] D. Frómeta, S. Parareda, A. Lara, S. Molas, D. Casellas, P. Jonsén, J. Calvo, Identification of fracture toughness parameters to understand the fracture resistance of advanced high strength sheet steels, *Eng. Fract. Mech.* 229 (2020) 106949.
- [112] S. Golling, D. Frómeta, D. Casellas, P. Jonsén, Influence of microstructure on the fracture toughness of hot stamped boron steel, *Mater. Sci. Eng. A* 743 (2019) 529–539.
- [113] Q. Lai, Z. Chen, Y. Wei, Q. Lu, Y. Ma, J. Wang, G. Fan, Towards the understanding of fracture resistance of an ultrahigh-strength martensitic press-hardened steel, *J. Mater. Res. Technol.* 27 (2023) 1996–2006.
- [114] E.E. Gdoutos, *Solid Mechanics and Its Applications*, 3rd ed., Springer, 2020.
- [115] J.R. Rice, A Path Independent Integral and the Approximate Analysis of Strain Concentration by Notches and Cracks, *J. Appl. Mech.* 35 (1968) 379–386.
- [116] D. Francois, A. Pineau, A. Zaoui, *Mechanical Behaviour of Materials: volume II: fracture mechanics and damage*, Springer Science & Business Media, 2012.
- [117] J.E. Burke, D. Turnbull, Recrystallization and grain growth, *Prog. Met. Phys.* 3 (1952) 220–292.
- [118] SSAB, Docol® PHS 1500 press hardening steel.
<https://www.ssab.com/en/brands-and-products/ssab-docol/automotive-steel-grades/press-hardening-steel/phs-1500> (accessed March 30, 2026).
- [119] SSAB, Docol® PHS 2000 press hardening steel,
<https://www.ssab.com/en/brands-and-products/ssab-docol/automotive-steel-grades/press-hardening-steel/phs-2000> (accessed March 30, 2026).

- [120] J. Schindelin, I. Arganda-Carreras, E. Frise, V. Kaynig, M. Longair, T. Pietzsch, S. Preibisch, C. Rueden, S. Saalfeld, B. Schmid, J.Y. Tinevez, D.J. White, V. Hartenstein, K. Eliceiri, P. Tomancak, A. Cardona, Fiji: An open-source platform for biological-image analysis, *Nat. Methods*. 9 (2012) 676–682.
- [121] ASTM E1820, Standard Test Method for Measurement of Fracture Toughness, ASTM, Annual Book of Standards. 3 (1820).
- [122] Plate bending test for metallic materials VDA 238-100, (2020).

Department of Engineering Sciences and Mathematics
Division of Materials Science

ISSN 1402-1544
ISBN 978-91-8142-032-6 (print)
ISBN 978-91-8142-033-3 (pdf)

Luleå University of Technology 2026